A new elasmosaurid (Sauropterygia, Plesiosauria) from the Bearpaw Shale (Late Cretaceous, Maastrichtian) of Montana demonstrates multiple evolutionary reductions of neck length within Elasmosauridae

DANIELLE J. SERRATOS,[1,2] PATRICK DRUCKENMILLER,[*,1,2] and ROGER B. J. BENSON[3]

[1]University of Alaska Museum, 907 Yukon Dr., Fairbanks, Alaska, 99775, U.S.A., serratos.danielle@gmail.com; psdruckenmiller@alaska.edu;

[2]Department of Geosciences, University of Alaska Fairbanks, Fairbanks, Alaska, 99775, U.S.A;

[3]Department of Earth Sciences, University of Oxford, Oxford U.K., OX1 3AN, rogerb@earth.ox.ac.uk

*Corresponding author

ABSTRACT—Plesiosauria is a diverse clade of marine reptiles that have been studied since the early 19th century. However, phylogenetic relationships within the group have been contentious due to limited taxon sampling and a misunderstanding of how ontogeny, interspecific and intraspecific variation affect character states. This is particularly true for elasmosaurids, a Cretaceous clade of long-necked plesiosaurians. In 2010, a new, nearly complete skeleton, MOR 3072, was collected from the Late Cretaceous (Campanian–Maastrichtian) Bearpaw Shale of northeast Montana. The specimen provides detailed morphological information rarely observed within Elasmosauridae, including a complete skull, the anterior 23 cervical vertebrae, a partial dorsal and caudal vertebral column, incomplete pectoral and pelvic girdles, elements of both fore- and hind limbs, ribs, and gastralia. Being early Maastrichtian in age, MOR 3072 is the stratigraphically youngest elasmosaurid known from the Western Interior Seaway, and is recognized as a new genus and species, *Nakonanectes bradti*. We present a description of *N. bradti* and conduct an extended phylogenetic analysis of Elasmosauridae. *N. bradti* is found to be deeply-nested within the clade of large-bodied, long-necked, Western Interior Styxosaurinae. However, MOR 3072 is one of the smallest adult elasmosaurids ever recovered (5.1–5.6 m) and exhibits a reduced neck length compared to other North American elasmosaurids, resulting from a reduction in both centrum length and number of cervical vertebrae (39–42 were originally present). These features are convergent with the Southern Hemisphere clade of short-necked Maastrichtian elasmosaurids, Aristonectinae, and demonstrate multiple origins of short-necked body proportions from longer-necked ancestors within Elasmosauridae.

INTRODUCTION

Plesiosauria is an extinct, monophyletic clade of secondarily aquatic Mesozoic marine reptiles. Plesiosaurians are fairly conserved with respect to their post-cervical body shape, but vary greatly in the relative proportions of skull size and neck length, ranging between two end-member morphotypes: the large-headed and short-necked pliosauromorphs and the small-headed and long-necked plesiosauromorphs (sensu O'Keefe and Carrano, 2005). Elasmosauridae is a derived plesiosaurian clade with plesiosauromorph body proportions, and elasmosaurids have classically been categorized as having a high number of cervical vertebrae with centra that are longer than dorsoventrally tall, elongated ilia, and humeri that are longer than femora (sensu Welles, 1952; Carpenter, 1999; Benson and Druckenmiller, 2014). Historically, a number of both Jurassic and Cretaceous plesiosauromorph genera have been included within Elasmosauridae (Carpenter, 1999; Gasparini et al., 2003; Großmann, 2007), but recent analyses restrict the clade to Cretaceous forms only (Sato, 2002; Kear, 2005; Ketchum and Benson, 2010; Benson and Druckenmiller, 2014). While the monophyly of Cretaceous Elasmosauridae is now well established, relationships within the clade are some of the least studied and most poorly understood among all plesiosaurians (Sato 2002; Ketchum and Benson, 2010; Benson and Druckenmiller, 2014; Sachs and Kear 2015; Araújo et al., 2015a; Otero et al., 2016), in part due to the lack of detailed understanding of the cranial anatomy of many taxa and the paucity of focused phylogenetic analyses of elasmosaurids. Nevertheless, attaining a consensus on elasmosaurid phylogeny is of fundamental importance for testing hypotheses about their

evolutionary history, including those regarding their high degree of variation in neck length (Otero et al., 2014a, 2016) and paleobiogeography (Mulder et al., 2000; Otero et al., 2012, 2015; Otero, 2016).

Elasmosaurids are globally distributed, having been found in Europe (Mulder et al., 2000; Sachs et al., 2016b), South America (Welles, 1962), Africa (Vincent et al., 2011; Lomax and Wahl, 2013), Australia (Sachs, 2004; Kear, 2005), New Zealand (Wiffen and Moisley, 1986; Cruickshank and Fordyce, 2002; Hiller et al., 2005), Asia (Sato et al., 2006; Sato et al., 2012) and Antarctica (O'Gorman et al., 2012, 2015). In North America, elasmosaurids are known from latest Cretaceous deposits along the west coast of California (Welles, 1943); however, the greatest diversity and actual number of specimens are found in Albian to Maastrichtian-aged deposits of the Cretaceous Western Interior Basin (WIB) (Welles, 1952; Carpenter, 1999). Based on current reviews, nine monotypic genera of elasmosaurids are recognized in the WIB (Welles, 1943; Carpenter, 1999; Sato, 2003; Druckenmiller and Russell, 2006; Kubo et al., 2012; Otero, 2016), although it is possible that species level diversity is greater still. Two genera from the Bearpaw Shale are the stratigraphically youngest-known forms from the WIB: *Terminonatator* (Sato, 2003) and *Albertonectes* (Kubo et al., 2012). The latter possesses 76 cervical vertebrae, the greatest count known in any vertebrate.

In the fall of 2010, a new, nearly complete skeleton of an elasmosaurid was discovered in the Bearpaw Shale of Montana, U.S.A. The specimen, MOR 3072, was found fully articulated and in situ at the bottom of a narrow ravine within the C. M. Russell National Wildlife Refuge (Fig. 1). At the time of discovery, much of the skeleton was preserved in a single large carbonate concretion, along with an articulated cervical

series extending into the outcrop, which was carefully documented in a series of field photos by the discoverer (Fig. 2). Unfortunately, the posterior half of the neck and anterior portion of the concretion were lost to erosion the following spring due to an intense runoff event. At the time of excavation, the anterior half of the cervical series and a complete skull were collected from the surrounding outcrop, along with the uneroded portion of the postcranial skeleton, which contained the posterior two-thirds of the coracoids, an unknown number of dorsal vertebrae, ribs and gastralia, anterior caudal vertebrae, portions of the left and right fore- and hind limbs, and much of the pelvic girdle (Fig 2).

MOR 3072 is significant in a number of respects. Stratigraphically, it is the youngest elasmosaurid described to date from the WIB and it possesses one of the shortest necks in terms of both cervical count and overall length of any elasmosaur known from North America. The quality of preservation in MOR 3072 also provides important new morphological data for elasmosaurids and permits the recognition of a new genus, described below. Finally, MOR 3072 is incorporated into a phylogenetic analysis using the largest existing phylogenetic data matrix of plesiosaurians, which helps to resolve poorly understood relationships within Elasmosauridae and elucidates aspects of neck length evolution in the clade.

Institutional Abbreviations—AMNH, American Museum of Natural History, New York, U.S.A.; **CM**, Canterbury Museum, Christchurch, New Zealand; **DM**, Museum of New Zealand Te Papa Tongarewa, Wellington; **DMNH**, Denver Museum of Natural History, Colorado, U.S.A.; **GMM**, Geomuseum, University of Münster, Germany; **KUVP**, Natural History Museum, University of Kansas, U.S.A.; **LACM**, Natural History Museum

of Los Angeles County, California, U.S.A. (previously housed at **CIT**, California Institute of Technology); **MOR**, Museum of the Rockies, Bozeman, Montana, U.S.A.; **NZGS**, New Zealand Geological Survey, Lower Hutt; **RSM**, Royal Saskatchewan Museum, Regina, Saskatchewan, Canada; **SDSMT**, South Dakota School of Mines and Technology, Rapid City, U.S.A.; **SMNK-PAL**, Staatliches Museum für Naturkunde Karlsruhe, Germany; **SMPSMU**, Shuler Museum of Paleontology, Southern Methodist University, Dallas, Texas, U.S.A.; **UAMES**, University of Alaska Museum Earth Sciences Collection, Fairbanks, Alaska, U.S.A.; **UCMP**, University of California Museum of Paleontology, Berkeley, U.S.A.

GEOLOGIC SETTING

The Western Interior Basin (WIB) of North America records numerous transgressive-regressive marine cycles of the epicontinental Cretaceous Western Interior Seaway (WIS) (Kauffman et al., 1993). During much of the Late Cretaceous the WIS extended north-to-south across the North American continent, from the Gulf of Mexico to the Arctic Basin (He et al., 2005) and had an estimated maximum depth of 200–500 m (Kauffman, 1984; Cobban et al., 2006).

The Bearpaw Shale was deposited during the Campanian and Maastrichtian and records the last transgressive-regressive cycle of the Western Interior Seaway (Kauffman et al., 1993). The Bearpaw Shale is an upper unit of the Montana Group and consists of dark clay shales with numerous calcareous concretions. The Bearpaw ranges between 60 m and 335 m thick (Cobban et. al., 2006; Feldmann et al., 2012),

although the vertical thickness at the discovery site of MOR 3072 was not measured. This westward-thinning tongue of marine shale disconformably overlies the Judith River Formation and is conformably overlain by the Fox Hills Sandstone in Montana (Feldmann et al., 1977; Condon, 2000) and the Eastend Formation in Canada (He et al., 2005). The Bearpaw Shale grades eastward into the Pierre Shale (Condon, 2000) and the outcrop similarity between the Bearpaw and Pierre shales makes these two units physically synonymous in the upper midcontinent of North America (Tourtelot, 1962; Feldmann et al., 2012).

The paleoenvironment of the Bearpaw Sea has been reconstructed using a number of different proxies. Dinoflagellates from the shale in central Montana suggest a low-salinity marine environment (Palamarczuk and Landman, 2011). This idea is further supported by freshwater algae associated with dinoflagellates (Palamarczuk and Landman, 2011; Cochran et al., 2003). The presence of diatoms may indicate a nutrient-rich and fertile Bearpaw Seaway (Bergstresser and Krebs, 1983). Paleotemperatures of the Bearpaw Sea have been estimated based on $\delta^{18}O$ and $\delta^{13}C$ values of molluscs to fluctuate between 12˚ and 19˚ C during the middle Maastrichtian (He et al., 2005).

Samples from the shale and concretion matrix surrounding MOR 3072 were analyzed for foraminifera and other carbonaceous material. The shale found around MOR 3072 is nearly pure mud with very little quartz and carbonaceous material. While foraminifera were absent, pyritized diatoms and glauconite grains were found in both the shale and concretion matrix that encased the specimen (pers. comm., M. Leckie) using a standard micropaleontological disaggregation method (Leckie et al., 1991).

Pyritized diatoms are commonly found in Late Cretaceous WIB strata (Bergstresser and Krebs, 1983) and indicate a seaway with rich primary production. We infer that MOR 3072 died in a relatively shallow marine environment with low sedimentation rate due to the absence of deltaic input or steady and significant freshwater influx from nearby shorelines.

The stratigraphic position of MOR 3072 within the Bearpaw was assessed on the basis of two ammonites recovered at the discovery site, which were identified as either *Baculites grandis* or *B. baculus* (pers. comm., J. Slattery and N. Landman). *B. grandis* (70.00 ± 0.4 Ma) and *B. baculus* (70.4 ± 0.5 Ma) indicate an early Maastrichtian age (He et al., 2005; Larson and Landman, 2007), which correlates to the *Endocostea typical*, *Inoceramus incurvus* and *Trochoceramus radiosus* Inoceramid Interval Zones of Cobban et al. (2006) and the Foraminiferal zone *Haplophragmoides excavate* (He et al., 2005). Thus, MOR 3072 is currently the youngest described Western Interior elasmosaurid, being younger than either of the other two Bearpaw Shale elasmosaurids, *Terminonatator* (Campanian *Baculites cuneatus–B. reesidei* zone) and *Albertonectes* (Campanian *B. compressus* zone) (Sato, 2003; Kubo et al., 2012).

METHODS

The skull and anterior half of the cervical series were preserved in a relatively soft shale, which was mechanically prepared using dental picks, air scribes, and air abrasive techniques. The preserved portion of the postcranial specimen was encased within a large carbonate concretion that was broken into smaller pieces in the field

before transport to UAMES for preparation. The concretionary block was both mechanically and chemically prepared using air scribes and repeated immersion in a 7% formic acid bath.

The skull of MOR 3072 was scanned using computed tomography (CT) at a medical facility; however, clear results were not obtained, possibly due to high levels of elemental barium (approximately 10%) detected using X-ray fluorescence. The skull and anterior four cervical vertebrae were also laser scanned into GeoMagic Studio 2013 with a Faro Edge at a resolution of 20 microns with a maximum point spacing of 50 microns. Ninety-four individual scan passes were collected with ~45% overlap resulting in 82,922,184 points that were globally aligned to a tolerance of less than 10 microns and surfaced with a maximum deviation of 10 microns and no subsampling of data. Two-dimensional TIFF files were developed through modification of these 3D files and presented in Figures 3 and 4 for a high-contrast, three-dimensional image of the skull.

SYSTEMATIC PALEONTOLOGY

DIAPSIDA Osborn, 1903

SAUROPTERYGIA Owen, 1860

PLESIOSAURIA de Blainville, 1835

XENOPSARIA Benson and Druckenmiller, 2014

ELASMOSAURIDAE Cope, 1869

STYXOSAURINAE Otero, 2016

Phylogenetic Definition—The clade including all taxa more closely related to *Styxosaurus snowii* than to *Aristonectes parvidens* (revised from Otero, 2016)

Comments—Otero (2016) recently erected the new subfamily Styxosaurinae for the clade of extremely long-necked elasmosaurids, which so far are known only from the Late Cretaceous of the Western Interior Seaway. He provided a phylogenetic definition delimiting the group that includes *Terminonatator*, *Styxosaurus* (including '*Hydralmosaurus'*), *Albertonectes*, *Elasmosaurus*, their most recent ancestor, and all its descendants. Since *Elasmosaurus* is a member of this clade by definition, then Styxosaurinae as defined by Otero (2016) is an objective junior synonym of Elasmosaurinae Cope, 1869 (subfamilies such as Elasmosaurinae are co-ordinate with families such as Elasmosauridae, therefore having identical authorities and dates; Article 36.1; ICZN, 1999).

However, although Otero (2016) recovered *Elasmosaurus platyurus* (the type species of *Elasmosaurus*) as a close relative of *Styxosaurus*, our phylogenetic analysis recovered *E. platyurus* as a wildcard taxon with uncertain affinities within Elasmosauridae (see below). This suggests two possibilities: (1) That the type specimen of *Elasmosaurus platyurus* may not be determinate at the subfamily level, in which case Elasmosaurinae can be abandoned; or (2) That *Elasmosaurus* may be less phylogenetically proximate to *Styxosaurus* than found by Otero (2016), in which case Styxosaurinae (sensu Otero [2016]; = Elasmosaurinae), is a larger and more inclusive clade than originally conceived, potentially even including Aristonectinae, in clear violation of the intended use of Styxosaurinae as a clade of primitively long-necked elasmosaurids and counterpoint to Aristonectinae (Otero, 2016).

A straightforward solution to this problem is to modify the phylogenetic definition of Styxosaurinae so that it does not use *Elasmosaurus* as an internal reference taxon. The emended definition given above refers only to a single internal specifier, which represents the type genus of Styxosaurinae, and to an external specifier for Aristonectinae, representing the only other formally defined subfamily within Elasmosaurinae (Otero et al., 2012). We note that if future studies find that *Elasmosaurus platyurus* belongs within 'Styxosaurinae', then Elasmosaurinae Cope, 1869 should be considered as a senior synonym of Styxosaurinae Otero, 2016.

NAKONANECTES gen. nov.

Type and Only Species—*Nakonanectes bradti*

Horizon—Bearpaw Shale, lower Maastrichtian, Upper Cretaceous

Diagnosis—As for the type and only species

NAKONANECTES BRADTI gen. et sp. nov.

(Figs. 2–14)

Holotype and Only Specimen—MOR 3072 including a complete skull, articulated anterior 23 cervical vertebrae, dorsal and anterior caudal vertebrae, partial coracoids, much of the forelimbs including partial humeri, complete epipodial and mesopodial rows and associated phalanges, both ilia and portions of the pubis and

ischium, portions of the hind limb including one complete and one partial femur with portions of the epipodial row and numerous ribs and gastralia.

Locality and Horizon—Near Fort Peck Reservoir, Phillips County, Montana within the Charles M. Russell National Wildlife Refuge. Precise coordinates of the discovery site are on file with the C. M. Russell National Wildlife Refuge office. Found in the *Baculites baculus–B. grandis* Zones of the Bearpaw Shale, lower Maastrichtian, Upper Cretaceous.

Etymology—The generic name is derived from *Nakona*, the name for native Assiniboine people of northeastern Montana, which means 'the friendly people'. The specific name honors David Bradt of Florence, Montana who found the specimen.

Diagnosis—*Nakonanectes bradti* is a small-bodied (estimated 5.1–5.6 meters long) elasmosaurid plesiosaurian (sensu Benson and Druckenmiller, 2014) with a proportionally short snout and short neck (39–42 cervical vertebrae), possessing the following autapomorphies that are unique among elasmosaurids: reduced, cordate external naris; prominent posteroventral process of maxilla projects ventral to the temporal bar and contacts squamosal posteriorly (this contact may also be present in '*Libonectes*' *atlasense* [pers. comm., S. Sachs September 2016], although this is difficult to confirm from our notes on the type specimen, which is poorly preserved in this region); posterior surface of ventral plate of basioccipital slopes anteroventrally; median contact of pterygoids posterior to posterior interpterygoid vacuity is anteroposteriorly short, revealing most of the ventral surface of the basioccipital in ventral view; posterolateral pterygoid lappet absent; deep anteroposteriorly-oriented

cleft in articular posterior to mandibular glenoid fossa; and small articular facets for preaxial accessory ossicles of the hind limb.

Nakonanectes bradti can further be diagnosed on the following unique character combinations: relatively short rostrum, with ratio of preorbital skull length to total skull length of 0.33; absence of a mandibular keel on the ventral surface of the symphysis; dorsomedially oriented premaxilla-maxilla suture; postfrontal participation in both the orbital and temporal margins; postorbital extends half the length of the ventral margin of the supratemporal fenestra; pineal slit level with postorbital bar; supraoccipital that is taller dorsoventrally than wide anteroposteriorly in lateral view; lateral surface of coronoid process comprised of dentary only; absence of lateral longitudinal ridge of the cervical vertebrae; lateral expansion of intercoracoid vacuity; and dorsal expansion of ilia twice the anteroposterior width of the midshaft.

DESCRIPTION

General Comments

MOR 3072 was found in articulation with the ventral surface of the body facing stratigraphically up. Much of the postcervical skeleton occurs in one large carbonate concretion (1.9 m long, ~1.0 m wide), while the skull and the proximal 23 cervical vertebrae were encased only in shale (Fig. 2). When it was first observed in the field, MOR 3072 preserved an estimated total of 39–42 cervical vertebrae, 16–19 of which were lost in a heavy spring runoff that occurred between the time of discovery and excavation. Small elasmobranch teeth and teleost scales are associated with the

skeleton along with a layer of macerated invertebrate material preserved stratigraphically below the postcranial elements within the concretion. Barite crystals are scattered around the postcranium but concentrated near the coracoid and acetabulum. A thin encrusting layer of pyrite is present on some bones and secondary barite mineralization occurs in both the bones and carbonate concretion.

The total adult body length of MOR 3072 is estimated at 5.1–5.6 m. In addition to the length of the skull (33 cm), preserved cervical series (0.9 m; Table 1), and length of the articulated block (1.2 m), the length of the missing portion of the posterior cervical vertebrae and anterior pectoral girdle, as well as the length of the missing posterior block (~0.2 m; Fig. 2), were estimated using field photographs (1.5 m). Tail length for MOR 3072 (0.99–1.48 m) was estimated based upon the percentage of tail to torso length in *Morenosaurus stocki* (163 cm / 200 cm = the tail is 82% the torso length; Welles, 1952), *Hydrotherosaurus alexandrae* (116 cm / 187 cm = 62%; Welles, 1952), and '*Hydralmosaurus*' *serpentinus* (= *Styxosaurus* sp.; AMNH 1495; 139 cm / 253 cm = 55%; Welles, 1952). MOR 3072 is interpreted to be an adult based upon the high degree of fusion of the atlas and axis, complete fusion of most neurocentral sutures and cervical ribs, and the advanced extent of ossification as seen in the complete articular contacts between propodial, epipodial, and mesopodial elements of the forelimbs (Brown, 1981).

Skull

The skull of MOR 3072 is complete but obliquely crushed laterally, with the mandible remaining articulated to the cranium (Figs. 2–4). The left side of the skull is

the best preserved (Fig. 3) and provides the basis for most interpretations of the skull roof. Only a small dorsolateral portion of the left squamosal is missing. The right side of the skull provides a partial view of the palate (Figs. 4–5).

MOR 3072 has a very short rostrum compared to other North American elasmosaurids (Sato, 2003). The beak index (percentage of preorbital region compared to the total skull length, as measured to the occipital condyle; Welles, 1952) is 33% for MOR 3072, similar to *Tuarangisaurus*, *Styxosaurus* sp. (AMNH 5835) and *Terminonatator ponteixensis* (35%; Wiffen and Moisley, 1986; Carpenter, 1999; Sato, 2003), *Zarafasaura* (31%: Vincent et al., 2011) and the aristonectine *Kaiwhekea katiki* (26%: e.g., Cruickshank and Fordyce, 2002) but much less than many other elasmosaurids, such as *T. ponteixensis*, which average 40% (Sato, 2003). This greatly shortened preorbital region results in a premaxilla-maxilla suture that is oriented nearly vertical in lateral view compared to *Styxosaurus snowii* and *Libonectes morgani,* both of which have sutures that are markedly inclined posteriorly (Williston, 1890; Welles, 1949; Sato, 2002). The supratemporal fenestra is large and measures 38% of the total skull length, close to the approximate value for *L. morgani*; however, the relative orbit to skull length is 17% in MOR 3072 and 22% in *L. morgani*, which falls within the range of variation noted for elasmosaurids in general (Araújo and Polcyn, 2013).

Dorsal Elements of the Skull—The premaxilla-maxilla contact, which is well sutured and difficult to discern, extends dorsally from the posterior margin of the fifth alveolus to the ventral margin of the ventral lobe of the external naris. The premaxilla forms the entire anterior and dorsal border of the external naris, which is uniquely

shaped like an inverted heart comprising anteriorly and a ventrally projecting lobes (Fig 3). This autapomorphic feature differs from the oval external naris seen in other elasmosaurids such as *Libonectes morgani* and *Hydrotherosaurus alexandrae* (Welles, 1943, 1949). Relative to overall skull size, the external naris is also conspicuously small compared to most elasmosaurids, with the exception of *Zarafasaura oceanis* (Vincent et al., 2011). The posteromedian process of the premaxilla contacts the medial margin of the frontal, just anterior to the premaxilla-parietal suture. The premaxilla-parietal suture appears deeply interdigitating, although this same region bears conspicuous anteroposteriorly elongate crenulations making it difficult to exactly demarcate the sutures. The premaxillae form a prominent and narrow dorsomedian ridge, which extends along their entire length and is most pronounced in the region dorsal to the external nares. However, the ridge does not appear to possess as sharp or prominent a mound or dorsomedian 'bump' as that seen in lateral view of *Styxosaurus snowii* (Sato, 2003). Numerous neurovascular foramina are located on the external surface of the premaxillae but the texture is generally smooth and lacks any prominent crests or ridges.

The left and right maxillae each bear 14 alveoli. In lateral view, the alveolar margin is slightly sigmoid in outline, with the anterior portion concave downward and the posterior portion convex, very similar to the alveolar margin of *Styxosaurus snowii* (KUVP 1301; Sato, 2002). The maxilla does not appear to contact the margin of the external naris, but the absence of a clear maxilla-prefrontal suture makes this relationship difficult to determine (Fig. 3). The maxilla has separated from the jugal along their suture on the left side, ventral to the orbit. Posteriorly, the maxilla narrows in

dorsoventral height and terminates posterior to the tooth row, ventral to the approximate midpoint of the lower temporal bar. The maxilla possesses a posteroventral process that extends from the ventral margin of the temporal bar and also forms a short contact with the squamosal. The presence of a prominent posteroventral process of the maxilla on the temporal bar, and the presence of a maxilla-squamosal contact are both autapomophies that are absent in all other elasmosaurids (e.g., Welles, 1943; Carpenter, 1997; Cruickshank and Fordyce, 2002; Sato, 2003; Vincent et al., 2011), with two possible exceptions: illustrations of *Terminonatator ponteixensis* (Sato, 2003:fig. 5) indicate the possible presence of a contact, although this region is obscured by a tooth and was not visible when viewed in person (D.J.S. pers. obs.); and a contact may be present in '*Libonectes*' *atlasense* (S. Sachs pers. comm., September 2016), although this region is poorly preserved in the type specimen and we were unable to confirm the presence of a contact using the notes from our examination of the specimen (R.B.J.B. pers. obs., SMNK-PAL 3978). In palatal view, the maxilla forms a portion of the lateral margin of the internal naris. Prominent, subpentagonal paradental plates form the medial margins of the alveoli. These have distinctively rugose medial surfaces that were described as a 'strong rugosity' in *Zarafasaura oceanis* (WDC CMC-01; Lomax and Wahl, 2013), and are widely present among plesiosaurians (e.g., Ketchum and Benson, 2011a; Benson et al., 2011), but are rarely noted in descriptions. In MOR 3072 the internal naris is located just posterior to the level of the external naris. This differs somewhat from the situation in *Libonectes morgani*, in which the posterior half of the internal naris overlaps with the anterior half of the external naris (Carpenter, 1997).

The orbit is roughly triangular with a slight anteroventral lobate extension, although this feature is not as well developed as that seen in some other elasmosaurids, including the holotypes of *Styxosaurus snowii* (KUVP 1301; Williston 1890) and *Tuarangisaurus keyesi* (Wiffen and Moisley, 1986). This extension is developed at least slightly in all elasmosaurids other than *Futabasaurus suzukii* (Sato et al., 2006) and the Early Cretaceous taxon *Eromangasaurus australis* (Sachs, 2004; Kear, 2005). In the absence of a discernable suture between the maxilla and prefrontal, our interpretation of the anterior orbit margin is uncertain. However, the prefrontal, or a descending process of the prefrontal, likely forms the anterior margin of the orbit and is interpreted to participate in the posterior margin of the external naris as is typical of elasmosaurids (Carpenter, 1997) (Fig. 3). If this interpretation is correct, then the prefrontal also shares a short contact with the premaxilla dorsal to the external naris. A well-defined interdigitating frontal-prefrontal suture is visible near the approximate midpoint of the anterodorsal orbital margin. The frontal forms the anterodorsal border of the orbital margin and its lateral margin is slightly convex and projects posteroventrally into the orbit. The boundaries of the postfrontal are difficult to interpret. However, the left postfrontal may be represented by a raised region forming the posterodorsal margin of the orbit. If this is correct, then the frontal-postfrontal suture is interpreted to lie along an apparent break between these two elements, where the postfrontal overlaps the frontal at the dorsal orbital margin. The interdigitating postfrontal-postorbital suture is also marked by a break near the posterodorsal margin of the orbit, a feature that is mirrored on both sides of the skull. Our interpretation of this region, in which the postfrontal is relatively large and participates in both the dorsal margin of the orbit and the anterior

margin of the temporal fenestra, differs from the condition observed in other Late Cretaceous elasmosaurids such as *Zarafasaura oceanis* (Vincent et al., 2011), *Hydrotherosaurus alexandrae* (Welles, 1943), and '*Libonectes*' *atlasense* (pers. obs., SMNK-PAL 3978). In these taxa, the postfrontal is small and only participates in the margin of the temporal fenestra, lacking any contribution to the orbit margin, a condition that represents a unique synapomorphy of a clade within Elasmosauridae (e.g., O'Keefe, 2001; Sato, 2002).

The postorbital forms the dorsal two-thirds of the posterior orbital margin. Anteriorly, the postorbital-jugal suture is visible at the orbital margin but is difficult to trace along its entire length posteriorly, where a change in bone-fiber orientation is the basis for delimiting the two bones. The posterolateral process of the postorbital is very long and forms approximately half of the ventral margin of the temporal fenestra, covering the entire dorsal border of the jugal dorsally, and thereby excluding the jugal from participating in the margin of the temporal fenestra. The jugal of MOR 3072 is broadly rectangular in shape with the anteroposterior axis being the longest. It forms the posteroventral margin of the orbit and is bordered ventrally by the maxilla along its entire anteroposterior length. The jugal-squamosal suture is subvertical, interdigitating, and occurs near the midpoint of the temporal bar. A small number of prominent foramina are visible on the jugal, and to a lesser extent, on the postorbital.

The anterior margin of the parietal lies immediately dorsal to the apex of the orbit, similar to the condition seen in *Libonectes morgani* (Welles, 1949; Carpenter, 1997), whereas in *Zarafasaura oceanis* and *Callawayasaurus colombiensis* the parietal-premaxilla suture lies posterior to this point (Welles, 1962; Vincent et al., 2011). A

distinct pineal foramen is not present although a narrow slit located at the anterior end of the parietal crest, immediately dorsal to the postorbital bar, may represent a remnant of this structure. Immediately anterior to and surrounding the pineal slit, the surface texture of the parietal bears numerous, small, anteroposteriorly-oriented ridges, but the surface texture becomes smooth posteriorly along the parietal crest. In lateral view, the dorsal margin of the parietal crest rises abruptly dorsally at its anterior end, but posteriorly it is oriented nearly horizontally. In contrast, in *Thalassomedon haningtoni* and *Styxosaurus snowii* the dorsal margin of the crest becomes progressively taller posteriorly and reaches its greatest height near its contact with the squamosal. In aristonectines such as *Kaiwhekea katiki* (Cruickshank and Fordyce, 2002; Benson and Druckenmiller, 2014) and in *Zarafasaura oceanis* (Vincent et al., 2011; Lomax and Wahl, 2013) the highest point of the parietal crest lies further anteriorly, due to the strong anterodorsal inclination of the suspensorium. In these taxa, the posterodorsal third of the supratemporal fenestra is bounded medially by the squamosal, thus differing markedly from MOR 3072 and many other elasmosaurids, in which the suspensorium is not as strongly inclined, and the entire medial margin of the temporal fenestra is formed by the parietal.

The suspensorium of MOR 3072 is inclined anteriorly at 15° from vertical. The dorsal processes of the squamosals extend laterally from their midline symphysis, which lies anterior to the occipital condyle, and then curve weakly posterolaterally. The squamosal symphysis is robust, rugose, and swollen so as to be convex dorsally, laterally and posteriorly forming a squamosal ‘bulb’ (sensu O’Keefe, 2001). Nevertheless, it is not swollen to the extent seen in *Styxosaurus snowii*, in which a more

prominent bulb projects posteriorly past the level of the suspensorium (KUVP 1301; D.J.S. pers. obs.). In posterior view, the ventromedial process of the squamosal is slightly less than half of the length of the quadrate shaft. The quadrate-squamosal suture is visible laterally, posteriorly and medially (Fig. 4). The quadrate ramus of the pterygoid contacts the pterygoid ramus of the quadrate along a distinct suture that is located posterior to the occipital condyle. The anterior ramus of the squamosal is bordered anteriorly by the postorbital dorsally and the jugal and maxilla ventrally.

Braincase—Portions of the epipterygoid, prootic, supraoccipital, exoccipital-opisthotic and basisphenoid can be seen in the left supratemporal fenestra (Fig 3). Elements of the lateral wall of the braincase are fully fused but most of their contacts can be traced by changes in bone fiber orientation. The left prootic is dorsoventrally taller than anteroposteriorly long and contacts both the anterior margin of the exoccipital-opisthotic and the anteroventral margin of the supraoccipital. The supraoccipital is approximately twice as tall dorsoventrally as wide anteroposteriorly. Due to crushing, the posterior surface of the supraoccipital is not visible, nor is the ventrolateral portion of the exoccipital-opisthotic; thus, foramina for exits of the cranial nerves cannot be seen. The paraoccipital process is longer than the dorsoventral height of the exoccipital-opisthotic and is mediolaterally narrower than dorsoventrally tall. Any lateral curvature of the paraoccipital process that may have been present is lost due to crushing. The posterior end of the paraoccipital process broadly contacts the quadrate and the squamosal. Because the pterygoid-quadrate suture is also clearly visible, there is a small but clear contact between the paraoccipital and pterygoid (Fig 4). The

paraoccipital process of MOR 3072 is interpreted to have inclined ventrally relative to the ventral surface of the exoccipital-opisthotic prior to taphonomic deformation.

The basioccipital bears a prominent ventral plate that differs from other elasmosaurids in being anteriorly inclined and therefore having a posterior surface that faces posteroventrally (Fig. 5). This contrasts with the vertical orientation seen in other elasmosaurids, such as *Libonectes morgani* (SMUSMP 69120). The ventral plate bears a weakly developed, dorsoventrally oriented midline ridge on its posterior surface, unlike the more prominent keel and deep lateral concavities seen in *Libonectes morgani* (SMUSMP 69120). In ventral view, the occipital condyle lies anterior to the quadrate condyle. Posteriorly, the occipital condyle is dorsoventrally taller than mediolaterally wide (2.9 cm by 2.4 cm) and is sub-rounded. The occipital condyle lacks a notochordal pit.

Palate—The anteromedial margin of the palatine forms the posterior border of the internal naris. The palatine closely approaches and may contact the other palatine along the midline as well as the posterior margin of the vomer. Likewise, the anterior ramus of the pterygoid also lies near and may contact the posterior margin of the vomer; however, the exact relationships among all three of these elements cannot be definitively discerned. Posteriorly, the palatine borders the anterior margin of the ectopterygoid.

The anterior interpterygoid vacuity is absent, similar to all other known elasmosaurids. A prominent pterygoid boss is located along the anterior margin of the subtemporal fenestra, two-thirds of which is formed by the lateral ramus of the pterygoid and one-third by the ectopterygoid. The pterygoid boss projects approximately 1 cm

ventrally from the palatal surface forming the anterior margin of the subtemporal fenestra. As preserved, it is anteroposteriorly longer than wide (length = 2.6 cm; width = 0.9 cm). Only the portion of this boss that is composed of the pterygoid is rugose along its ventral surface. Although somewhat flattened taphonomically, the ventral surfaces of the pterygoids are anteroposteriorly 'dished' lateral and anterior to the posterior interpterygoid vacuity, similar to condition seen in other elasmosaurids (e.g., *Callawayasaurus colombiensis*; *Libonectes morgani*; D.J.S. pers. obs., SMUSMP 69210; UCMP 38349), and in leptocleidians (e.g., O'Keefe 2001; Druckenmiller and Russell 2008). This morphology is a synapomorphy of Xenopsaria (Elasmosauridae + Leptocleidia) that is also present in some rhomaleosaurids (Benson and Druckenmiller 2014). The medial processes of the pterygoids posterior to the posterior interpterygoid vacuity are anteroposteriorly narrow, and appear to share only a small contact along the midline. This configuration is unique among elasmosaurids, and results in exposure of the ventral surface of the basioccipital anterior to the median suture of the pterygoids (immediately posterior to the posterior interpterygoid vacuity; Figs. 4 and 5). In contrast, the medial processes of the pterygoids of other non-aristonectine elasmosaurids, including *L. morgani* (Carpenter, 1997), *C. colombiensis* (Welles, 1962), and *Zarafasaura oceanis* (Vincent et al., 2011) are anteroposteriorly broader and meet along the midline in a broad contact that leaves only a small portion of the basioccipital visible posteriorly, and entirely covers the ventral surface of the basioccipital anteriorly. The pterygoid configuration of MOR 3072 also contrasts to that seen in aristonectines such as *Alexandronectes zealandiensis*, in which a posteromedial contact of the pterygoids is absent (Otero et al., 2016). MOR 3072 lacks a posterolateral pterygoid lappet ventral to

the quadrate ramus of the pterygoid. This structure is present in other elasmosaurids where this region is visible, such as *L. morgani* (O'Keefe, 2001) and *C. colombiensis* (P.S.D. pers. obs., UCMP 38349).

The pterygoids are split medially by the cultriform process of the parasphenoid at the anterior end of the posterior interpterygoid vacuity. The ventral surface of the cultriform process is flat anteriorly but then develops a narrow median keel posteriorly along most of the length of the posterior interpterygoid vacuity. A posteriorly-oriented process, approximately 7 mm long, extends from the ventral margin of the parasphenoid keel, ventrally underlapping the anterior end of the basioccipital. This process is also present in *L. morgani* (Carpenter, 1997), although it is slightly less prominent. The midpoint of the posterior interpterygoid vacuity is posterior to the anterior margin of the subtemporal fossa. Within the posterior interpterygoid vacuity the parasphenoid underlaps the basisphenoid; posteriorly it may also underlap part of the basioccipital just anterior to the medial processes of the pterygoids, although the exact location of the element is equivocal.

Mandible—There are 19 alveoli in the left dentary, 18 in the right, and three alveoli adjacent to the mandibular symphysis. There is a conspicuous absence of a symphyseal keel on the ventral surface of the mandible, unlike *Styxosaurus* (SDSMT 451; Carpenter, 1999) and *Thalassomedon haningtoni* (DMNH 1588). The symphyseal region is pitted in a manner consistent with that of the premaxillae. In lateral view, the dentary varies in dorsoventral height due to a slight sigmoid curvature of the tooth row, which is deepest anteriorly at the symphysis, and posteriorly just anterior to the coronoid eminence. The dentary extends 69% of the anteroposterior length of the entire

mandibular ramus. The extent of bowing of the mandibular ramus is not possible to determine due to taphonomic distortion. The left coronoid process (=eminence) is not visible laterally, but the posterior margin of the right process can be seen medial to lower temporal bar, and its outline is indicated by a dashed line in Figure 4. The coronoid process is very prominent, and rises nearly vertically from the surangular-dentary contact, which lies along the posterior margin of the process. Thus, the coronoid process is formed entirely by the dentary, similar to that seen in *Styxosaurus snowii* (KUVP 1301) but differing from *Libonectes morgani*, in which the coronoid process is low and the surangular and dentary contribute equally. In MOR 3072, the anterior margin of the coronoid process is not visible, but the posterior margin is tall and slightly concave posteriorly, suggesting that the overall shape is very similar to the narrowly triangular morphology seen in *Terminonatator ponteixensis* (Sato, 2003).

In lateral view, the posterior margin of the dentary is formed along a subvertical suture that lacks a prominent posterior projection into the surangular-angular contact. The surangular contacts the angular along a straight suture just ventral to the ventral margin of the mandibular fossa. The anterodorsal surface of the retroarticular process bears a deep anteroposteriorly-oriented cleft that lies immediately posterior to the mandibular fossa (Figs. 3–4). This cleft is not present in any other described elasmosaurids but is present in most leptocleidians (Ketchum and Benson, 2010) and in the Early Jurassic plesiosaurian *Stratesaurus taylori* (Benson et al., 2015). The retroarticular process of MOR 3072 is anteroposteriorly longer than the mandibular fossa and is dorsoventrally taller than wide in cross section, being mediolaterally widest in its dorsal half. The dorsoventral orientation of the retroarticular process is nearly

horizontal and is slightly deflected medially in dorsal view. The posterior surface of the retroarticular process is concave. The retroarticular processes of *Thalassomedon haningtoni* (DMNH 1588) and *Styxosaurus snowii* (KUVP 1301) are very similar in overall shape, curvature and orientation to those of MOR 3072, while *Callawayasaurus colombiensis* (UCMP 38349) has a proportionally smaller retroarticular processes.

Elements of the medial surface of the mandible are best exposed on the left ramus (Figs 4, 5). The anterior margin of the splenial participates in the mandibular symphysis, but the angular does not. The splenial is bordered ventrally by the angular in the region between the 6th to the 13th alveoli and posteriorly by the prearticular. The splenial terminates posteriorly at the anterodorsal edge of the posterior opening for the Meckelian canal. The angular-prearticular contact extends posteriorly from its anterior end ventral to the 14th dentary alveolus, to a zone of slightly rugose bone ventral to the mandibular glenoid fossa. The angular-prearticular suture is not tightly fused along its entire length; rather it is separated by two slit-like foramina directly ventral to the Meckelian canal. The posterior opening for the Meckelian canal is an elongate (50 cm), slit-like structure with a well-defined, curving anterior margin that is inclined at approximately 30 degrees from the horizontal. This is similar to the condition seen in other elasmosaurids (Sato, 2002), including *L. morgani* (Carpenter, 1997), but lacks the essentially vertical anterior margin seen in *Terminonatator* (Sato, 2003). The Meckelian canal is bordered ventromedially by the prearticular, dorsally by the surangular, and posteriorly by the articular just anterior to the mandibular fossa.

Hyoids—Both hyoids were recovered from the palatal region of the skull during preparation (Fig. 6). The right hyoid was discovered encased in shale matrix at the

posterior end of the skull, ventral to medial processes of the pterygoid. The left hyoid was located ventral to the palatine, suggesting slight taphonomic displacement. The hyoids are sigmoidal in overall shape. The anterior and posterior ends of the hyoids are slightly convex, the anterior of which is larger in diameter. An anteroposteriorly-oriented sulcus occurs along the length of the shaft beginning and ending approximately 1 cm before the anterior and posterior margins. Elements of the hyoid apparatus are rarely preserved in elasmosaurids and have only been noted in *Eromangasaurus* (Kear, 2005), *Callawayasaurus colombiensis* (Welles, 1962) and *Aristonectes quiriquinensis* (Otero et al., 2014a).

Dentition—The teeth of MOR 3072 are curved both distally and lingually. Most teeth are also gently inclined anteriorly but cannot be described as procumbent. Tooth size varies dramatically along the tooth row. The anterior teeth are relatively small compared to more posterior teeth, but the first premaxillary tooth is not significantly smaller than the third, unlike in *Hydrotherosaurus alexandrae* (UCMP 33912), and *Terminonatator ponteixensis* (Sato, 2003) where the first premaxillary tooth is much smaller than any other premaxillary teeth. A reduced first premaxillary alveolus is in fact widespread among plesiosauroids (Sato, 2002; Benson and Druckenmiller 2014:character 140), including early elasmosaurids such as *Callawayasaurus colombiensis* and *Eromangasaurus australis* (Welles, 1962; Sachs, 2004; Kear, 2005;), but is absent in most Late Cretaceous elasmosaurids, including *Libonectes morgani* (Carpenter, 1997), *Styxosaurus snowii* (KUVP 1301) and *Zarafasaura oceanis* (Vincent et al., 2011). The largest caniniform teeth are located along a mediolaterally broad portion of the tooth row that includes the posterior portion of the premaxilla and the

anterior third of the maxilla. In the posterior half of the tooth row, the dentary teeth are consistently larger than their corresponding maxillary teeth, a trait visible on both sides of the skull, and shared with many other elasmosaurids, as discussed by Buchy (2005). Teeth of the upper and lower tooth rows generally display a deeply interdigitating relationship with one another, with the exception of two pairs of adjacent teeth (the third and fourth left maxillary teeth and the eighth and ninth right maxillary teeth) that lack a gap to accommodate an intervening dentary tooth. A similar relationship is seen in some tooth positions of *Callawayasaurus colombiensis* and *Libonectes morgani* (Welles, 1949, 1962; Carpenter, 1997).

The teeth of MOR 3072 are D-shaped in cross-section at the base of the crowns, with the labial surface being flat, a distinctive dental morphology that is widespread among Late Cretaceous elasmosaurids (Welles, 1943; Sato, 2002). There are enameled ridges concentrated on the medial, lingual and distal surfaces of both upper and lower crowns, though none are observed on the labial surface. Some ridges extend straight from the base to the mid-point of the crown and converge or terminate apically, while other ridges occur only at the base. Significant wear facets are seen on the eighth and ninth left maxillary teeth as well as the ninth right maxillary tooth and the eighth dentary tooth.

Axial Skeleton

The collected portion of the cervical series includes 23 vertebrae, all but one of which (number 23) were found in articulation. The total number of missing cervicals in MOR 3072 (excluding pectorals) was estimated from counts taken off of multiple

photographs of the complete skeleton taken at the time of discovery. Fifteen additional vertebrae can be clearly counted in the field photographs, all of which have ventrolaterally-positioned, sub-circular rib facets. The number of remaining cervicals that are wholly contained within the concretion are estimated by extrapolation from the last clearly visible vertebra (38) to the approximate anterior edge of the pectoral girdle, the location of which was determined by the placement of the coracoids following preparation. We estimate that the first pectoral vertebra would be dorsal to the anterior half of the scapulae based upon articulated skeletons of *Albertonectes vanderveldei*, *Hydrotherosaurus alexandrae*, and *Morenosaurus stocki* (Welles, 1943; Kubo et al., 2012). One or two vertebrae seen emerging from the cliff may also have been lost to erosion. Hence, we estimate as few as 39 to as many as 42 cervical vertebrae in total. Absolute neck length is estimated at 2.2 m (excluding skull) based upon comparisons of the posterior preserved cervical vertebrae, pectoral girdle, and forelimb elements to photographs of the complete skeleton. Thus, MOR 3072 has both the fewest total number of cervical vertebrae of any known North American elasmosaurid and the shortest adult neck in terms of relative and absolute length (see Discussion below). It may also possess the lowest vertebral count of any elasmosaurid. *Morenosaurus stocki*, a short-necked elasmosaurid from the Maastrichtian of California, has 46 cervical vertebrae (Welles, 1943), and aristonectines also possess short necks with estimated counts of approximately 43 vertebrae (Cruickshank and Fordyce, 2002; Otero, 2016; although only 37 cervical vertebrae are preserved in *Aristonectes quiriquinensis*; Otero et al., 2014a).

Atlas-Axis Complex—Sutures of the atlas-axis complex are closed except those of the axial neural arch. As is typical for elasmosaurids, the atlantal centrum does not participate in the anterior margin of the atlantal cup, being excluded by the atlantal neural arch (Fig. 7). In anterior view, the atlantal centrum is visible and deeply recessed within the atlantal cup, but does not extend to the lateral margin of the atlantal cup. In lateral view, a small foramen (described as a 'pit' by Kubo et al. [2012] for *Albertonectes vanderveldei*) is situated between the base of the atlantal and axial neural spines, which are fused dorsally. Ventrally, the atlas-axis complex bears a prominent hypophyseal ridge that originates on the anterior half of the atlantal centrum and extends posteriorly along most of the length of the axial centrum, similar to *Vegasaurus molyi* (O'Gorman et al., 2015). Ventral to the atlas, the ridge is mediolaterally broad and flat ventrally, but it becomes sharply keeled ventral to the axis. The neural spine slopes posterodorsally at approximately 25–30 degrees, similar to *Thalassomedon haningtoni* and *A. vanderveldei* (Welles, 1943; Kubo et al., 2012). Both the atlas and axis possess distinct ribs that are separate proximally but fuse distally (Fig. 7). The axial and atlantal ribs are broken in most elasmosaurid specimens we have examined. However, the morphology seen in MOR 3072 is also present in *Tuarangisaurus keyesi* (Wiffen and Moisley, 1986), *Thalassomedon hanningtoni* (Carpenter, 1997), *Aristonectes quiriquinensis* (Otero et al., 2014a), and *Albertonectes vanderveldei* (Kubo et al., 2012) and is likely to be widespread among elasmosaurids. The atlantal ribs extend posterior to the posterior margin of the axis centrum.

Postaxial Cervical Series—All of the collected cervical centra are mediolaterally wider than anteroposteriorly long (as measured along the posterior face) and

dorsoventrally taller than long (Table S1, Fig. 8). Based upon field photographs, the posterior cervical vertebrae are also mediolaterally wider than anteroposteriorly long, although the relative dorsoventral height is difficult to determine. The anteroposteriorly short cervicals differ markedly from the elongated anterior to middle cervicals of *Terminonatator ponteixensis*, *Styxosaurus snowii*, *Albertonectes vanderveldei* and *Elasmosaurus platyurus* (Sato, 2003; Sachs, 2005; O'Keefe and Hiller, 2006; Otero, 2016). The Vertebral Length Index (VLI) for cervical vertebrae 3–23 ranges from 74.7–99.7 (mean = 90.8). By comparison, other Western Interior elasmosaurids such as *Thalassomedon haningtoni*, *Libonectes morgani*, *Styxosaurus snowii*, *Terminonatator ponteixensis*, SDSMT 451, and *E. platyurus* have mean VLIs ranging between 103–138 (O'Keefe and Hiller, 2006). However, short cervicals with mean VLIs closest to that of MOR 3072 are *Aristonectes quiriquinensis* (80; Otero et al., 2014a) and *Hydrotherosaurus alexandrae* (97; Welles, 1943), both of which also happen to be Maastrichtian elasmosaurids.

In posterior view, a weakly developed ventral notch is present in the third cervical which becomes increasingly better developed and more conspicuous by vertebra nine (Fig. 8). Centra 10–23 are clearly binocular-shaped due to the presence of a prominent ventral notch. In posterior view, as seen in photographs, the posterior cervicals have broad ventral notches that diminish in size posteriorly along the series. All preserved cervicals have a shallow groove that parallels the perimeter of the articular surfaces of the centra, similar to *Hydrotherosaurus alexandrae and T. ponteixensis*. The prominence of this feature in MOR 3072, which is clearly an adult, suggests it is not

solely a juvenile characteristic (Brown, 1981; Ketchum and Benson, 2010; Benson and Bowdler, 2014).

Unlike most North American elasmosaurids (e.g., Sato, 2002), MOR 3072 lacks a lateral longitudinal ridge on all preserved cervicals, similar to the aristonectine *Kaiwhekea katiki*, and to *Futabasaurus suzukii* (Cruickshank and Fordyce, 2002; Sato et al., 2006). A rugosity is present along the lateral articular surfaces of the centra, immediately anterior and posterior to the rib facets, beginning at cervical nine. Posteriorly, the rugosity becomes more pronounced and expands dorsally along the articular rims; this is clearly visible in field photographs of posterior cervicals. Anterior cervical rib facets are subcircular but become slightly anteroposteriorly longer throughout the preserved series beginning at cervical 20. Anterior rib facets are situated slightly posteriorly on the centra, but shift to a more central position in posterior cervicals. *Morenosaurus stocki* similarly retains subcircular rib facets throughout its cervical series (Welles, 1943), unlike the middle to posterior cervicals of *S. snowii* and *A. vanderveldei* that have distinctly anteroposteriorly elongate facets (D.J.S. pers. obs., KUVP 1301; Kubo et al., 2012). A narrow ventral median keel is present in vertebrae 3–7 and becomes a well-developed, mediolaterally broad and rounded ventral ridge in more posterior centra. A ventral ridge is also visible in vertebrae from the posterior half of the cervical series, although it is difficult to determine if the ridges were rounded or flat from photographs. Diminutive (2–5 mm long) paired subcentral foramina are present in all cervicals.

The neural arches are firmly fused to the centra throughout the entire preserved series but the neurocentral sutures remain clearly visible. Neural arch facets are

rectangular and extend almost the length of the dorsal surface of the centra unlike the aristonectine TTU P 9219, which has smaller, oval shaped facets (Chatterjee and Small, 1989). Dimensions of the neural arches and spines from the missing posterior cervicals are unknown. The left and right pre- and postzygapophyses are all fused along the midline; however, they do not fuse along their entire length so that in dorsal view the anterior margins of prezygapophyses (and posterior margin of postzygapophyses) are U-shaped in outline, similar to *A. vanderveldei* (Fig. 8; Kubo et al., 2012). Each prezygapophyseal facet is mediolaterally concave, with the fused left and right facets producing a U-shaped trough in anterior view. Postzygapophyseal facets are similarly convex. Numerous tiny pits are clustered on the anteroventral surface of prezygapophyses and on the posterior surface of neural arches ventral to the postzygapophyses. Neural spines of the anterior 23 cervical vertebrae are shifted posteriorly, such that the anterior margins of neural spines are collinear with the midpoint of their respective centra. In lateral view, the dorsal margins of neural spines slope anteriorly at approximately 10 degrees from vertical, and the anterior margins of neural spines are concave. In *Zarafasaura oceanis* (Lomax and Wahl, 2013) and '*Libonectes' atlasense* (Buchy, 2005) the cervical neural spines also slope anteriorly but at a much steeper angle (~45 degrees). In lateral view, the third and fourth neural spines are taller than long, cervical spines 5–9 are approximately equidimensional and spines 11–21 are longer than tall. Neural spines do not exceed the heights of their respective centra in the preserved cervicals and neural spine length increases proportionally faster than height. The posterior margins of the neural spines are convex overall, with a rugose, posteriorly projecting process at spine mid-height beginning at

cervical four and becoming more pronounced throughout the series. *Cardiocorax mukulu* also bears a posterior projection near mid-height of the neural spine (Araújo et al., 2015a) but differs from MOR 3072 in also possessing an anteriorly projecting process.

Almost all anterior cervical ribs (3–7 and 13–21) are fused to their centra, although the sutures are clearly visible. In cervical vertebrae 8–12 however, ribs are unfused and fully separated from the centra. As is visible in field photographs, all posterior cervical ribs are also unfused and displaced. Anterior-most cervical ribs bear a dorsolaterally positioned ridge along most of their length, resulting in a triangular cross-sectional view of ribs 4–10. Gradually, the ridge reduces its length distally so that it becomes primarily an anteroposteriorly-oriented ridge at the midlength of ribs 11–21 (Fig. 8). These more posterior ribs are thickest in their proximal half and thinnest distally. Rib morphology posterior to cervical 21 is unknown. In lateral view, the preserved cervical ribs have a conspicuous distal expansion that is weakly developed anteriorly and strongly developed posteriorly beginning at cervical four, similar to those of *T. haningtoni* (DMNH 1588). In ribs 15–21, the anteroposterior length of the distal rib margin is greater than the dorsoventral length of the ribs.

Dorsal vertebrae—Interpretations of the dorsal series are based on three prepared vertebrae: two anterior dorsals located adjacent to the coracoid and one middle dorsal centrum (Fig. 9). The dorsal centra are anteroposteriorly short compared to the height and width of the centra, which are approximately equal in dimension (Table S1). The transverse processes of all three dorsals are situated more ventrally on the neural arches relative to *Hydrotherosaurus alexandrae* (Welles, 1943). The transverse

processes of the anterior dorsals are inclined dorsally at 20–25 degrees from the horizontal and angled slightly posteriorly. The cross-sectional shape of the transverse processes is subcircular, with somewhat flattened ventral surfaces. The diameter of the distal articular facet of the transverse process is approximately twice the diameter mid-shaft. The articular facets for the dorsal ribs are rounded in lateral view, convex, and face posteroventrally. The preserved dorsal neural spine is approximately equal in height to its respective centrum. MOR 3072 displays a faint anteroposterior constriction along the base of the neural spines, similar to the condition seen in most other elasmosaurids (e.g., Welles, 1943, 1962; Benson and Druckenmiller, 2014:character 183), but in contrast to *Albertonectes vanderveldei*, which has none (Kubo et al., 2012). In lateral view, the neural spines are roughly rectangular in shape and mediolaterally thin (9.2 cm tall, 0.6 cm wide and 5.5 cm long in the best preserved spine). Other data regarding the number and morphology of dorsal vertebrae will be available once preparation of the large concretionary block is complete.

Caudal vertebrae—Five partially prepared and articulated caudal vertebrae are visible in MOR 3072, likely from the anterior portion of the tail. However, the total number of caudal vertebrae is unknown (Fig. 10). Centra have a length to width ratio of 1.3–1.6, which differs significantly from that of *Styxosaurus* sp. (AMNH 1495) and *Hydrotherosaurus* (0.6–0.8). Rib facets are located approximately at the mid-height of centra and are circular in outline. Notably, the rib facets project strongly laterally, similar to *Kawanectes lafquenianum*, a feature that was previously considered diagnostic for that taxon (O'Gorman, 2016a). The chevron facets are located exclusively along the posteroventral margin of the centrum, similar to *A. vanderveldei* (Kubo et al., 2012), and

are not shared between adjacent centra as in *Styxosaurus* sp. (AMNH 1495; Welles, 1943 as '*Hydralmosaurus*'). The location and prominent size of the chevron facets produce a sharply angled ventral centrum margin in posterior view. Two parallel, anteroposteriorly-oriented ridges are located along the ventral surface of the centrum, similar to *Hydrotherosaurus alexandrae* (Welles, 1943). One or two pairs of ventral foramina are located medial and/or lateral to the ventral ridges. All of the preserved caudal ribs are unfused with the centra. The caudal ribs are dorsoventrally flattened, bear a slight anteriorly-projecting process about mid-length, and are approximately equal in length to the width of their corresponding centra in the preserved series. A single disarticulated chevron is preserved that curves posteriorly in lateral view (Fig. 10).

Appendicular Skeleton

Coracoids—The clavicular arch, scapulae, and anterior third of the coracoids (including the glenoid fossae, anteromedial process of the coracoid and margins of the pectoral fenestrae) were lost to erosion; however, the posterior two-thirds of the coracoids were collected and the ventral surface prepared (Fig. 11). The left and right coracoids are not fused but remain in articulation with only a small area of contact ventrally along the midline, leaving a broad V-shaped gap in anterior view between each symphyseal facet (Fig. 11A). Whether this relationship between the left and right coracoids was partly or wholly present in life (and presumably filled with connective tissue) or simply a result of dorsoventral compression is unclear. A prominent, ventral transverse ridge extends from the approximate location of the glenoid fossa (although

this is missing) toward the midline. An anteroposteriorly short, ventrally-projecting, median process is present where the transverse ridges merge along the midline. The ventral process appears to have extended 5 centimeters from the base of the blade and was smoothly rounded before being damaged in the field. Similar ventral projections are widespread among elasmosaurids (e.g., Welles, 1943; Sato, 2002:character 167) and early xenopsarians including *Brancasaurus brancai* and *Vectocleidus pastorum* (Wegner, 1914; Benson et al., 2012), and vary in their morphology. For example, the ventral process of MOR 3072 is less pronounced than the very prominent ventral process seen in the Early Cretaceous elasmosaurids *Wapuskanectes betsynichollsae* (Druckenmiller and Russell, 2006). The outline of the intercoracoid vacuity is cordate and similar in shape to, but proportionally larger than, that of *Callawayasaurus colombiensis* (Welles, 1962). The posterolateral cornu extends at least as far laterally as the glenoid fossa and possibly further, based upon the placement of the left humeral head as seen in field photographs (Fig. 2), similar to *Hydrotherosaurus alexandrae, C. colombiensis, and W. betsynichollsae*. Although MOR 3072 is an adult, the coracoids do not meet posterior to the intercoracoid vacuity, as seen in *W. betsynichollsae* (Druckenmiller and Russell, 2006). The posterior margins of the coracoid blades are broadly convex in ventral view, similar to most elasmosaurids, but proportionally larger and more bulbuous, rather than being fan-shaped as in *C. colombiensis* (Welles, 1962). MOR 3072 also displays a proportionally larger gap between the left and right posterior coracoid blades than that exhibited by *Libonectes morgani* (Welles, 1949).

Forelimbs—Portions of both forelimbs are preserved in MOR 3072. The left forelimb consists of preaxial portions of the distal humerus, the articulated radius and a

partial intermedium. The right forelimb, which is more complete, includes the distal third of the humerus, the complete epipodial, mesopodial, and the metapodial rows as well as portions of seven proximal phalanges (Fig. 12). Humeral length is estimated at 39–41 cm, based upon data extrapolated from field photographs of the left side. Maximum distal width (as measured on the right humerus) is approximately 55% of midline length, compared to 79% in *Vegasaurus molyi* (O'Gorman et al., 2015), 73% in *Wapuskanectes betsynichollsae* (Druckenmiller and Russell, 2006), 68% in *Kawanectes lafquenianum* (O'Gorman, 2016a), 64% in *Terminonatator ponteixensis* (Sato, 2003) and 64–65% in *Futabasaurus suzukii* (Sato et al., 2006). Thus, the humerus is relatively longer and narrower than other described North American elasmosaurids. Distally, the preaxial margin of the distal humerus is slightly convex. The entire distal end of the humerus is separated into two facets, a large radial facet (68% of total distal width) and a smaller ulnar facet (32%). The radial facet of MOR 3072 is proportionately much larger than that seen in *T. ponteixensis* (56%) and *F. suzukii* (50–52%). Both facets are concave and angled at 155 degrees relative to each other where they meet. In many Late Cretaceous elasmosaurids the radial and ulnar facets of the humerus are both relatively deeply concave so that the anterior portion of the radial facet and posterior portion of the ulnar facet are oriented in approximately the same plane as each other (Sato, 2002:character 198). However, a different morphology is present in MOR 3072, *Albertonectes*, *Styxosaurus* ('*Hydralmosaurus*'), *Hydrotherosaurus*, and *Terminonatator*, which have straight ulnar facets (Welles, 1943; Sato, 2005; Kubo et al., 2012).

The preaxial margin of the radius and the postaxial margin of the ulna are straight. The radius is anteroposteriorly wider than proximodistally long (14.5 cm and 13

cm, respectively) and has a clearly defined articular facet for the radiale and intermedium. A well-formed epipodial foramen is present and less than half the length of the epipodials. The ulna is equal in proximodistal length to the radius, but it is roughly 75% the width of the radius and has well-formed facets for the intermedium, ulnare, and the proximal accessory ossicle.

Two postaxial accessory ossicles are present: the proximal, which is incomplete, lies between the epipodial and proximal mesopodial row and the distal ossicle, which is complete, lies between the proximal and distal mesopodial rows and contacts metapodial V. It is unclear if a third postaxial accessory ossicle articulated to the humerus and proximal end of the ulna, similar to that observed in *Morenosaurus stocki* (Welles, 1943). The distal accessory ossicle is smaller than metacarpal V and possesses well-defined articular surfaces for the ulnare and metacarpal V. The distal mesopodial row contains carpals 1, 2, 4, and metacarpal V, which has shifted proximally into the postaxial margin of this row. Carpals 2 and 3 articulate with the radiale and intermedium; carpal 4 articulates with both the intermedium and ulnare. The proximal margins of metacarpals II and III are bi-faceted for articulation with both mesopodial 1 and 2, and 2 and 4, respectively.

Only the proximal ends of the first row of phalanges are articulated in the right forelimb; however, more distal phalanges are visible and semi-articulated in the block containing the caudal vertebrae (Fig. 10). MOR 3072 displays an interlocking pattern between adjacent digits, unlike *Futabasaurus suzukii* (Sato et al., 2006), *Albertonectes vanderveldei* (Kubo et al., 2012), and *Terminonatator ponteixensis* (Sato, 2003), although only the proximal phalanges are preserved in *T. ponteixensis*. All preserved

phalanges are less than twice as long as wide, similar to other elasmosaurids such as *A. vanderveldei* and *F. suzukii* (Sato et al., 2006).

Ilia—Both ilia are preserved and the right is completely prepared (Fig. 13). Because the pelvic girdle is largely articulated (although slightly compressed), it is possible to determine the relative position and orientation of the ilia with confidence. For orientation purposes, we refer to the sacral end of the ilium as dorsal and the acetabular end as ventral. In dorsal view, the dorsal end of the ilium is anteroposteriorly elongate and a rugosity is visible along the concave medial surface where the sacral rib facet is located. In medial view, the dorsal margin is slightly wider than the ventral margin (6.3 cm and 5.9 cm, respectively), but in anterior view the dorsal margin is approximately half the width of the ventral margin (4 cm and 8.2 cm, respectively). In lateral view, the dorsal portion of the ilium is separated from the anteriorly and laterally curving ventral half by a posteriorly projecting eminence or 'knee', similar to CM Zfr 159 (1994.91.1) (Hiller et al., 2014). The long axis of the ilium is slightly angled in either lateral or medial view, but is not as strongly angled as that observed in *Vegasaurus molyi* (O'Gorman et al., 2015). The cross-sectional shape at the midpoint of the shaft is subtriangular with the flat surfaces facing medially and posterolaterally and a subrounded face directed anteriorly. The acetabular facet occupies roughly 70% of the ventral surface of the ilium and faces anterolaterally, while the ischial facet is approximately 30% of the ventral surface of the ilium and faces posterolaterally. The edge between the acetabular and ischial facets is a hummocky protrusion that does not extend up the shaft of the ilium, in contrast to the groove that extends between the facets and into the shaft of the non-aristonectine Chilean elasmosaurid SGO.PV.6506 (Otero et al., 2014b).

Hind Limbs—Only the proximal third of the right femur is preserved, while the left hind limb is represented by a complete femur, the dorsomedial half of the tibia and a small fragment of the fibula. The maximum width to midline length of the left femur is 57% compared to 63% in *Terminonatator ponteixensis* (Sato, 2003) and 64–71% in *Futabasaurus suzukii* (Sato et al., 2006). In preaxial view, the femur is concave dorsally and convex ventrally (Fig. 14). The femur is approximately 75% the length of the humerus. Both femora preserve a hummocky capitulum and trochanter that are constricted along the pre- and postaxial surfaces but are broadly connected along the epiphyseal surface. The trochanter faces posterodorsally, is located directly dorsal to the capitulum, and is not offset pre- or post-axially. The insertion for the adductor musculature is located ventrally along the proximal third of the diaphysis where it is deeply rugose. The cross-sectional shape of the femur at this rugosity is subcircular with a flattened ventral margin. In dorsal view, the tibial facet of the femur appears straight but is slightly concave in ventral view. The left distal propodial margin is separated into two shallow facets, a large tibial (73% of total distal length) and smaller fibular facet (27%). For comparison, the total distal length of facets on the femur of *T. ponteixensis* is 59% tibial and 41% fibular and for *F. suzukii* it is 48% tibial and 52% fibular (Sato, 2003; Sato et al., 2006). The tibial facet is more concave than the shallow fibular facet and they are angled at 150 degrees relative to each other.

The tibia is approximately 78% the width of the radius. A small articular facet, possibly for an accessory ossicle (not preserved), is located along the distal preaxial margin of the femur and continues onto the proximal margin of the tibia. The presence of preaxial accessory ossicles in the hind limb has not been documented in any known

elasmosaurid. The presence of an epipodial foramen is equivocal. The proximal margin of the tibia has a squared articular margin with the propodial, in contrast to the rounded convex margin of *Terminonatator ponteixensis* (Sato, 2003). In ventral view, the preaxial half of the tibia is depressed but this artifact is attributed to taphonomic crushing.

PHYLOGENETIC ANALYSIS

Taxon Sample and Data Sources

We modified the matrix of Benson and Druckenmiller (2014), resulting in a matrix of 270 characters and 92 taxa (Supp. Data 1), by adding *Nakonanectes bradti* (MOR 3072) and twelve additional elasmosaurid OTUs: *Albertonectes vanderveldei* (Kubo et al., 2012)*, Aristonectes quiriquinensis* (Otero et al., 2014), *Elasmosaurus platyurus* (Cope, 1869; Welles, 1952; Everhart, 2005; Sachs, 2005), '*Hydralmosaurus serpentinus*' (= *Styxosaurus* sp.; Otero et al., 2016), *Mauisaurus haasti* (based on examination of TPM R1529, CM Zfr 115, and information in Hector [1874] and Hiller et al. [2005]), '*Libonectes*' *atlasense* (SMNK-PAL 3978; Buchy, 2005), *Styxosaurus snowii* (KUVP 1301; Williston, 1890; Sato, 2002), *Terminonatator ponteixensis* (RSM P2424.1; Sato, 2003), *Tuarangisaurus keyesi* (NZGS CD 425, 426; Wiffen and Moisley, 1986), and *Zarafasaura oceanis* (Vincent et al., 2011; Lomax and Wahl, 2013), as well as two recently reported small-bodied elasmosaurids from the Southern hemisphere *Kawanectes lafquenianum* (O'Gorman, 2016a) and *Vegasaurus molyi* (O'Gorman et al., 2015).

Our matrix includes 22 definite elasmosaurids, plus *Gronausaurus wegneri* (based on examination of GWWU A3.B2 and information in Hampe, 2013) and *Brancasaurus brancai* (GWWU A3.B4; Wegner, 1914), which may be either basal elasmosaurids or basal leptocleidians (e.g., Wegner, 1914; Benson and Druckenmiller, 2014; Otero et al., 2016). Compared to previous analyses, this represents the largest analysis of elasmosaurids to date: Otero (2016) included 19 elasmosaurids plus *Brancasaurus*, and excluded *Gronausaurus*, and O'Gorman (2016a) included 18 elasmosaurids plus *Brancasaurus* and *Gronausaurus*. Our matrix includes three taxa not analyzed by either of those two studies: *Nakonanectes bradti*, '*Libonectes*' *atlasense*, and *Zarafasaura oceanis*; plus two more taxa not analyzed by Otero (2016: *Kawanectes lafquenianum* and *Vegasaurus molyi*) and by O'Gorman (2016a: '*Hydralmosaurus serpentinus*' [= *Styxosaurus* sp.] and *Mauisaurus haasti*). Because the elasmosaurids in our dataset were scored independently of the works by Otero (2016) and O'Gorman (2016a), we believe it is valuable as an independent attempt to infer the phylogenetic relationships among elasmosaurids. In fact, many of our key results are shared with those of Otero (2016; see below), and this builds towards a broader consensus on elasmosaurid relationships.

Because complete and reliable anatomical data have not yet been published for all elasmosaurids, and because we have not personally examined all specimens, we could not include all the taxa analyzed by Otero (2016) or O'Gorman (2016a) in our analysis. Two of the OTUs analyzed by O'Gorman (2016a) are therefore absent from the current study: *Thalassomedon hanningtoni* and *Morenosaurus stocki* (Welles, 1943). Two of the OTUs analyzed by Otero (2016) are also absent from the current

study: *Thalassomedon haningtoni* and the aristonectine *Alexandronectes zealandiensis* (Otero et al., 2016); and two are represented within more inclusive OTUs: *Styxosaurus browni* (AMNH 5835), which is included in our '*Hydralmosaurus serpentinus*' OTU following the taxonomic framework of Carpenter (1999) (AMNH 1495; = *Styxosaurus* sp. according to Otero, 2016), and *Morturneria seymourensis* (Chatterjee and Small, 1989), which is included in our *Aristonectes parvidens* OTU following Gasparini et al. (2003). Because these pairs of taxa are highly similar and phylogenetically proximate (Otero et al., 2016), the use of these composite OTUs in our analysis should have a minimal effect on the resulting topology.

Our matrix also incorporates a critical reexamination of recently published scores for *Libonectes morgani* (Sachs and Kear, 2015). Sachs and Kear (2015) re-coded many of the scores for this taxon that were presented in our previous analysis (Benson and Druckenmiller, 2014). This provides an opportunity for reappraisal of our character descriptions and interpretations of the anatomy of *L. morgani*. We find that 44% (28 out of 64) of their suggested re-codings are justified, and a detailed discussion, with photographs provided as evidence for the scores used in this analysis is provided in Supplementary Data 2.

Character List

We modified the character list of Benson and Druckenmiller (2014) in two ways. Firstly, we added a new character state (2) to character 139 describing the sub-oval cross-section of elasmosaurid teeth (e.g., Welles, 1943).

Secondly, we added a new state (3) to character 153, which describes the highly elongate proportions of the cervical central of some Late Cretaceous elasmosaurids (O'Keefe and Hiller, 2006; Otero, 2016; *Terminonatator, Styxosaurus*, *Elasmosaurus* and *Albertonectes*; Williston, 1890; Sato, 2003; Sachs, 2005; O'Keefe and Hiller, 2006; Otero et al., 2016; Kubo et al., 2016). This morphology was quantitatively demonstrated and described as 'elongate' (O'Keefe and Hiller, 2006) or 'can-shaped' with the anteroposterior length of middle cervical centra greater than their mediolateral width (Otero et al., 2016), despite the presence of mediolaterally broad cervical centra in elasmosaurids. The taxa that show this character state have especially long middle cervical centra and high variability in proportional centrum length along the cervical series (O'Keefe and Hiller, 2006). The revised descriptions of these two characters are as follows:

139. Cross-sectional shape of teeth in anterior half of tooth row: round or sub-rounded (0); sub-triangular (1); sub-oval (2).

153. Proportions of anterior–middle cervical centra: substantially shorter than high [length <0.7 x height] (0); approximately as long as high (1); substantially longer than high (2).

We also corrected the descriptions of two characters as follows:

25. Maxilla and dentary, posterior extent of tooth row: around orbital midlength or more anteriorly (0); ventral to postorbital bar (1); ventral to temporal fenestra midlength (2) (this previously referred only to the maxillary tooth row).

248. Humerus, angle between long axes of epipodial facets in dorsal view: oblique (0); close to 180 degrees (1) (this previously described the 'propodials' instead of just the humerus).

Tree Searches

Initial tree searches were conducted in PAUP*4.0b10 (Swofford, 2002) using the parsimony ratchet (Nixon, 1999) implemented by PAUPRat (Sikes and Lewis, 2001) to find a population of 95 most parsimonious trees (MPTs; length = 1450 steps; CI = 0.2705; RI = 0.6839). This was then explored using TBR branch swapping until a large set of trees was recovered (>75,000 trees). The strict consensus of these trees includes an only partly resolved Xenopsaria, in which many elasmosaurids form a polytomy with Leptocleidia and two elasmosaurid subclades: (1) Aristonectinae (sensu Ketchum and Benson, 2011; Otero et al., 2011) comprising *Kaiwhekea katiki*, *Aristonectes quiriquinensis* and *Aristonectes parvidens*; and (2) a clade comprising '*Hydralmosaurus serpentinus*' (= *Styxosaurus* sp.), *Styxosaurus snowii*, and *Nakonanectes bradti*. The lack of resolution within Elasmosauridae results from the presence of wildcard taxa that occupy several different positions among the set of MPTs: *Eromangasaurus australis*, *Elasmosaurus platyurus*, and *Futabasaurus suzukii*. Therefore, we implemented a strict reduced consensus approach (Wilkinson, 2003) to resolving elasmosaurid relationships, by pruning those taxa from the set of MPTs prior to computing a strict consensus. Wildcard taxa were identified manually by examining the set of MPTs, and by computing Adams consensus.

Pruning *Eromangasaurus australis* from the set of MPTs resulted in a reduction to 55,630 unique trees, and the resolution of Elasmosauridae as the sister taxon of Leptocleidia, plus the Speeton Clay plesiosaurian as the sister taxon of all other elasmosaurids in the strict reduced consensus. *Gronausaurus wegneri* was found in a polytomy with Elasmosauridae and Leptocleidia, underscoring uncertainties about its precise phylogenetic affinities (compare Hampe [2013] with Benson and Druckenmiller [2014]). This seems to demonstrate that *G. wegneri* is an important, phylogenetically basal taxon that likely embodies key information on plesiomorphic character states, regardless of its precise affinities among early xenopsarians. We therefore disagree with the decision of Otero (2016) to exclude it from their analyses.

Pruning *Elasmosaurus platyurus* resulted in a further reduction to 51,372 unique trees and resolution of a large, inclusive clade comprising *Mauisaurus haasti*, *Kawanectes lafquenianum* and *Vegasaurus molyi* in a polytomy with a clade of *Hydrotherosaurus alexandrae* (*Albertonectes vanderveldei*, *Terminonatator ponteixensis*, (*Nakonanectes bradti*, ('*Hydralmosaurus serpentinus*' (= *Styxosaurus* sp.), *Styxosaurus snowii*))). This differs from the topology found by Otero (2016), in which Styxosaurinae included only *Albertonectes vanderveldei*, *Terminonatator ponteixensis*, '*Hydralmosaurus serpentinus*' (= *Styxosaurus* sp.), *Styxosaurus snowii* (of those taxa analyzed here), with *Hydrotherosaurus alexandrae* found outside of the clade comprising Aristonectinae + Styxosaurinae. Our topology differs from that of O'Gorman (2016a), who found members of Styxosaurinae (sensu Otero [2016] and herein) dispersed across the tree as a polyphyletic assemblage of long-necked elasmosaurids. Similar to our results, O'Gorman (2016a) also found *K. lafquenianum* and *V. molyi* as

close relatives to each other. However, whereas we found them within Styxosaurinae, O'Gorman (2016a) found them as close relatives of Aristonectinae.

Pruning *Futabasaurus suzukii* resulted in a further reduction to 48,356 unique trees and resolution of *Libonectes morgani* and *Zarafasaura oceanis* in a polytomy outside of Aristonectinae, and '*Libonectes*' *atlasense* and *Tuarangisaurus keyesi* as successively more proximate sister taxa of the clade comprising Aristonectinae + Styxosaurinae. The presence of *T. keyesi* outside of Aristonectinae + Styxosaurinae is similar to the results of Otero (2016), who also found *L. morgani* in this region of the tree, differing from our topology.

We believe that the finer-scale differences between our topology and that of Otero (2016) result from the relative incompleteness of comparative anatomical work on elasmosaurids compared to that for other plesiosaurians, and future anatomical study may resolve the contentious areas of elasmosaurid phylogeny. Nevertheless, our topology has several major features in common with that of Otero (2016), in particular the recovery Aristonectinae, and of Styxosaurinae as a clade that includes long-necked, Western Interior Seaway elasmosaurids. The following section focuses on character support for that clade, as character support for Aristonectinae has already been discussed by Otero et al. (2012), Benson and Druckenmiller (2014), and Otero (2016).

Character Support of Styxosaurinae

Our topology suggests that Styxosaurinae is a more inclusive clade than that found by Otero (2016), which only included taxa with extremely elongated cervical centra from the Late Cretaceous Western Interior Seaway of North America. Our

topology suggests inclusion of several taxa that lack extremely elongated cervical centra within Styxosaurinae (although these taxa still have high counts of cervical vertebrae): the Late Cretaceous southern hemisphere taxa, *Kawanectes lafquenianum*, *Mauisaurus haasti*, *Vegasaurus molyi*, and *Hydrotherosaurus alexandrae*, from the Maastrichtian of the west coast of California.

Styxosaurinae is supported by seven unambiguous synapomorphies in our analysis: (1) squamosal bulb present (58.1; unique among elasmosaurids); (2) notochordal pit present on occipital condyle (63.1; unique among Late Cretaceous elasmosaurids, but also present in *Callawayasaurus*; Welles, 1949); (3) anterior cervical neural spines inflected/oriented anterodorsally (157.2; also present in *Aristonectes quiriquinensis*; Otero et al., 2014); (4) low count of dorsal vertebrae (17–19; 179.0; unique among elasmosaurids, and the higher count seen in *Vegasaurus* [O'Gorman et al., 2015] is a reversal); (5) low count of pectoral vertebrae (2–4; 180.0; also present in *Futabasaurus* [Sato, 2006]); (6) femoral trochanter narrow and projects dorsally (253.0; unique among Late Cretaceous elasmosaurids, but present in *Callawayasaurus* [Welles, 1949]; and transformed to state 1 in *Albertonectes* [Kubo et al., 2012]); (7) epipodial foramen present but small, proximodistal diameter less than half of epipodial length (261.1; although note that many elasmosaurids are polymorphic between the forelimb and hind limb for this character). Otero (2016) described the low count of dorsal vertebrae (179.0) as being plesiomorphic, and stated that it was present in *Futabasaurus suzukii*. However, Sato et al. (2006:fig. 2) and our examination of a cast of the type specimen at NHMUK indicate a count of at least 21 dorsal vertebrae in *F.*

suzukii, and the low dorsal vertebral count is found as a unique synapomorphy of Styxosaurinae among elasmosaurids.

We also recover several potential synapomorphies of Styxosaurinae under DELTRAN (character states 142.1, 209.2, 227.1 and 45.0) and ACCTRAN (character states 68.0, 69.1, 78.1, 84.1, 102.0, 103.3 and 111.1).

The clade comprising *Hydrotherosaurus alexandrae* and all more derived styxosaurines is supported by unambiguous synapomorphies: (1) middle caudal chevron facets project significantly ventrally (193.1; unique among elasmosaurids, but reversed to low chevron facets in *Nakonanectes*); (2) epipodial facets of humerus oriented at an oblique angle to each other (248.0; also present in *Callawayasaurus* and *Wapuskanectes*; Welles, 1962; Druckenmiller and Russell, 2006), which is unique among Late Cretaceous elasmosaurids, in which the facets are usually oriented at 180° to each other (Sato, 2002). We also recover a further potential synapomorphy of this clade under DELTRAN (220.1) and ACCTRAN (64.0).

The clade of styxosaurines with elongate cervical centra and extremely long necks (*Albertonectes vanderveldei*, '*Hydralmosaurus serpentinus*' (= *Styxosaurus* sp.), *Styxosaurus snowii*, *Terminonatator ponteixensis*), plus *Nakonanectes bradti* is supported by five unambiguous synapomorphies: maxillary dentition highly heterodont (133.1; also present in *Libonectes morgani* and '*Libonectes*' *atlasense* among elasmosaurids; Carpenter, 1997; Buchy, 2005), highly 'elongate' or 'can-shaped' morphology of cervical centra, especially middle cervical centra (153.3; unique among plesiosaurians; reversed in *Nakonanectes bradti*), anterolateral cornu of pubis present, extending further laterally than the acetabulum (230.1; unique among elasmosaurids),

femoral length to width ratio between 1.55 and 2.00, showing more elongate proportions than those of other elasmosaurids (251.2; also present in *Futabasaurus*; Sato et al., 2006); mediolateral width of tibia more that 10% greater than that of the fibula (265.0; unique among elasmosaurids). Additional possible synapomorphies are recovered under ACCTRAN (115.1, 152.6, 190.0, 191.0, 201.1, 205.0 and 232.1).

DISCUSSION

Elasmosaurid relationships are currently in a state of flux. Recent analyses (Araújo et al., 2015a; 2015b; Sachs and Kear, 2015; O'Gorman, 2016; Otero et al., 2014a; Otero, 2016; Otero et al., 2016) have attempted to address this problem but there has been little congruence between analyses in part due to the use of different data matrices (O'Keefe and Street, 2009; Ketchum and Benson, 2010; Benson and Druckenmiller, 2014) as well as poor taxon sampling, and a paucity of thorough descriptive data in the literature.

Recently, Otero (2016) conducted a large phylogenetic analysis of elasmosaurids, adding 13 new elasmosaurid OTUs to the Benson and Druckenmiller (2014) matrix. The analyses presented here was conducted independently, and provides an opportunity to initiate a consensus on the major features of elasmosaurid phylogeny. Both analyses were broadly similar in recovering a basal grade of Early Cretaceous forms, and two, apparently stable, Late Cretaceous clades: Aristonectinae and Styxosaurinae (Fig. 15). Styxosaurinae (sensu Otero, 2016) consists of Campanian, Western Interior elasmosaurids all of which exhibit extreme neck

elongation, including some of the longest necks of any known plesiosaurians, including *Albertonectes* (Kubo et al., 2012) and possibly *Elasmosaurus* (our analysis did not support the inclusion of *Elasmosaurus* in Styxosaurinae).

The topology presented by O'Gorman (2016a) differs more substantially. Specifically, the topology among other non-aristonectines was not fully resolved and differs in most respects from those of both Otero (2016) and the present study. Nevertheless, it recovered the small-bodied southern hemisphere taxa, *Kawanectes lafquenianum* and *Vegasaurus molyi* as close relatives (O'Gorman, 2016), together with *Morenosaurus stocki*, a relatively short-necked taxon from the Maastrichtian of California (which was not included in our analysis).

Our results have several implications regarding elasmosaurid evolution. They suggest that cervical number within Elasmosauridae is more labile than previously appreciated. In a more traditional concept of the clade, elasmosaurids are distinguished by high cervical counts (typically greater than 55) and elongate cervical centra (Welles, 1943; 1952). However, recent analyses have clarified the phylogenetic position of *Aristonectes*-like taxa within Elasmosauridae (Ketchum and Benson, 2011b; Benson and Druckenmiller, 2014; Otero et al., 2014a), considerably expanding the elasmosaurid morphological concept to include as few as 37 cervical vertebrae (a minimum estimate for *Aristonectes quiriquinensis* based on the number preserved; Otero et al., 2014a) and considerably anteroposteriorly shortened centra. The discovery of *Nakonanectes bradti* indicates a second independent evolution of short necks within Elasmosauridae, surprisingly nested within Styxosaurinae, the clade that includes the longest-necked elasmosaurids. This underscores the fact that there was not a simple, single trend

within Elasmosauridae toward increasingly longer necks over time. Various selective pressures possibly relating to feeding ecology, locomotion and possibly even sexual selection produced a mosaic of head size, neck lengths, and torso proportions throughout their long evolutionary history of at least 65 million years (O'Keefe and Hiller, 2006).

Aristonectines, *Zarafasaura*, and MOR 3072 all possess short snouts, and relatively short necks with low vertebral counts and proportionally short centra (although they are shortest in aristonectines). The evidence so far indicates that these features were acquired convergently and represent homoplasy. MOR 3072 can be readily distinguished from aristonectines and *Zarafasaura* by many differences described above, especially in the morphology of the suspensorium (e.g., the presence of a squamosal bulb in MOR 3072; the presence of a strongly anterodorsally inclined squamosal arch with an anteriorly-pointing V-shaped outline when seen in dorsal view in aristonectines and *Zarafasaura*). In consequence, we find strong support for the inclusion of MOR 3072 in a clade of otherwise long-necked Western Interior Seaway elasmosaurids from the Northern Hemisphere, and not with aristonectines, from equivalent-aged (Campanian–Maastrichtian) strata of the Southern Hemisphere. Therefore, short-necked elasmosaurids evolved independently in the Northern and Southern hemispheres during the latest Cretaceous. Furthermore, the small body size of *Nakonanectes* was acquired independently of small body size in the Southern hemisphere taxa *Vegasaurus* (O'Gorman et al., 2015) and *Kawanectes* (O'Gorman 2016a: estimated body length = 3.8 m compared to 5.1–5.6 m in *Nakonanectes*).

Recently, O'Gorman (2016b) redescribed the type material of *Fresnosaurus drescheri* (LACM 2758; Welles, 1943) along with previously undescribed postcranial material catalogued under the same number. This latter material, not considered to actually be part of the *Fresnosaurus* type specimen, was referred by O'Gorman (2016b) to Aristonectinae indet. on the basis of the morphology of a pectoral centrum that he used as a proxy for the proportions of the posterior cervical centra, which are not preserved. If this referral (an admittedly "weak determination"; O'Gorman, 2016b:18) is correct, it represents the first evidence for Aristonectinae in the Northern Hemisphere. However, the recognition of non-aristonectines likes *Nakonanectes bradti* with relatively short and wide cervical centra and a ventral notch calls into question this identification and suggests that cervical morphology alone is not a reliable character for referral to Aristonectinae, as was recently suggested by Sachs et al. (2016a) in the description of new elasmosaurid material from Sweden.

Another taxon with a relatively reduced cervical count is *Morenosaurus stocki* Welles, 1943, from the Maastrichtian Moreno Formation of California. *Morenosaurus* is known from two specimens (LACM 2802 and LACM 2749), the latter of which preserves a complete series of 46 cervical vertebrae as well as a partial skull and first pectoral vertebra (Welles, 1943). However, we did not include *Morenosaurus* in the current analysis because we were not able to examine the anatomy in sufficient detail. Therefore, the systematic relationships of *Morenosaurus* taxa to *Nakonanectes* remain untested.

Bearpaw Shale Elasmosaurids

The holotype specimen of *Nakonanectes bradti*, MOR 3072, was recovered from the lower Maastrichtian units of the Bearpaw Shale. Based on ammonite biostratigraphy, *Nakonanectes* represents the youngest occurrence of any elasmosaurid from both the Bearpaw Shale and the Western Interior Basin, being 2–3 million years younger than *Terminonatator* ponteixensis (Campanian *Baculites cuneatus–B. reesidei* zone) and 3–4 million years younger than *Albertonectes vanderveldei* (Campanian *B. compressus* zone) (Sato, 2003; Kubo et al., 2012). It is interesting to note that both the longest (*A. vanderveldei*; 76 cervicals), and shortest (*Nakonanectes*; 39–42 cervicals) necks of non-aristonectine elasmosaurids are from the same geologic formation, within a relatively short interval of time, and also belong to the same clade, Styxosaurinae. *Nakonanectes* is the third described elasmosaurid from the Bearpaw Shale, one of few Cretaceous elasmosaurids with detailed skull and postcranial osteology available for study, and one of the smallest adult elasmosaurids yet discovered. *Nakonanectes* provides evidence that elasmosaurid diversity remained high near the waning stages of the clade's long temporal duration throughout most of the Cretaceous. Its surprisingly short neck, in terms of both absolute length and cervical count, also bear witness to the remarkable morphological disparity in the clade, which has traditionally been renowned primarily for its dramatic neck elongation.

ACKNOWLEDGMENTS

We are indebted to David Bradt, who found MOR 3072 and provided the photo in Fig. 2, and his family, without whom this study would not have been possible. Our

sincere thanks go to B. Skinner and the staff at the C. M. Russell National Wildlife Refuge, as well as the volunteers that helped excavate the specimen. UPS and Lynden Transport donated the shipping costs for the specimen from Montana to Alaska. We thank M. Leckie (University of Massachusetts Amherst), J. Slattery (University of South Florida), N. Landman (American Museum of Natural History), M. Sliwinski and K. Severin (University of Alaska Fairbanks). J. Pruitt and the Idaho Visualization Laboratory laser scanned and made 3D reconstructions of the skull; L. Watson and Fairbanks Memorial Hospital provided CT scans. At UAF, we acknowledge P. McCarthy, S. Fowell, J. Van Veldhuizen, J. Rousseau, A. Edgar, E. Boone, M. Shay, L. Gangloff, H. Foss, T. Martz and E. Nadin. The manuscript benefited from constructive reviews by S. Sachs and an anonymous reviewer. This study was part of a Masters thesis completed at the University of Alaska Fairbanks.

LITERATURE CITED

Araújo, R., and M. J. Polcyn. 2013. A biomechanical analysis of the skull and adductor chamber muscles in the Late Cretaceous plesiosaur *Libonectes*. Palaeontologia Electronica 16:1–25.

Araújo R., M. J. Polcyn, A. S. Schulp, O. Mateus, L. L. Jacobs, A. Olímpio Gonçalves, and M. -L. Moirais. 2015a. A new elasmosaurid from the early Maastrichtian of Angola and the implications of girdle morphology on swimming style in plesiosaurs. Netherlands Journal of Geosciences 1–12.

Benson, R. B. J., and T. Bowdler. 2014. Anatomy of *Colymbosaurus megadeirus* (Reptilia, Plesiosauria) from the Kimmeridge Clay Formation of the U.K., and high diversity among Late Jurassic plesiosauroids. Journal of Vertebrate Paleontology 34:1053–1071.

Benson, R. B. J., and P. S. Druckenmiller. 2014. Faunal turnover of marine tetrapods during the Jurassic–Cretaceous transition. Biological Reviews 89:1–23

Benson, R. B. J., K. T. Bates, M. R. Johnson, and P. J. Withers. 2011. Cranial anatomy of *Thalassiodracon hawkinsi* (Reptilia, Plesiosauria) from the Early Jurassic of Somerset, United Kingdom. Journal of Vertebrate Paleontology 31:562-574.

Benson, R. B. J., H. F. Ketchum, D. Naish, L. E. Turner. 2012. A new leptocleidid (Sauropterygia, Plesiosauria) from the Vectis Formation (Early Barremian–early Aptian; Early Cretaceous) of the Isle of Wight and the evolution of Leptocleididae, a controversial clade. Journal of Systematic Palaeontology 11:233–250.

Benson, R. B. J., M. Evans, and M. A. Taylor. 2015. The anatomy of *Stratesaurus* (Reptilia, Plesiosauria) from the lowermost Jurassic of Somerset, United Kingdom. Journal of Vertebrate Paleontology DOI: 10.1080/02724634.2014.933739.

Bergstresser, T. J., and W. N. Krebs. 1983. Late Cretaceous (Campanian-Maastrichtian) diatoms from the Pierre Shale, Wyoming, Colorado and Kansas. Journal of Paleontology 57:883–891.

Blainville, H. D. de. 1835. Description de quelgues espéces de reptiles de la Californie. Nouvelles Annales du Muséum d'Histoire Naturelle, Paris 4:233–296.

Brown, D. S. 1981. The English Upper Jurassic Plesiosauroidea (Reptilia) and a review of the phylogeny and classification of the Plesiosauria. Bulletin of the British Museum (Natural History) Geology Series 35:253–344.

Buchy, M. -C. 2005. An elasmosaur (Reptilia: Sauropterygia) from the Turonian (Upper Cretaceous) of Morocco. Carolinea 63:5–28.

Carpenter, K. 1997. Comparative cranial anatomy of two North American Cretaceous plesiosaurs; pp. 191–216 in J. M. Callaway and E. L. Nicholls (eds.), Ancient Marine Reptiles. Academic Press, San Diego, California.

Carpenter, K. 1999. Revision of North American elasmosaurids from the Cretaceous of the Western Interior. Paludicola 2:148–173.

Chatterjee S., and B. J. Small. 1989. New plesiosaurs from the Upper Cretaceous of Antarctica. Geological Society Special Publication 47:197–215.

Cobban, W. A., K. C. McKinney, J. D. Obradovich, and I. Walaszczyk. 2006. USGS zonal table for the Upper Cretaceous Middle Cenomanian-Maastrichtian of the Western Interior of the United States Based on ammonites, inoceramids, and radiometric ages. U.S. Geological Survey Open-File Report 2006-1250:1–45.

Cochran, J. K., N. H. Landman, K. K. Turekian, A. Michard, and D. P. Schrag. 2003. Paleoceanography of the Late Cretaceous (Maastrichtian) Western Interior Seaway of North America: evidence from Sr and O isotopes. Palaeogeography, Palaeoclimatology, Palaeoecology 191:45–64.

Condon, S. M. 2000. Stratigraphic framework of Lower and Upper Cretaceous rocks in central and eastern Montana. US Geological Survey 303:236–1535.

Cope, E. D. 1869. Extinct Batrachia, Reptilia and Aves of North America. Transactions of the American Philosophical Society 14:1–252.

Cruickshank A. R. I., and R. E. Fordyce. 2002. A new marine reptile (Sauropterygia) from New Zealand: further evidence for a Late Cretaceous Austral radiation of cryptoclidid plesiosaurs. Palaeontology 45:557–575.

Druckenmiller, P. S., and A. P. Russell. 2006. A new elasmosaurid plesiosaur from the Early Cretaceous Clearwater Formation, northeastern Alberta, Canada. Paludicola 5:184–199.

Druckenmiller, P. S., and A. P. Russell. 2008. A phylogeny of Plesiosauria (Sauropterygia) and its bearing on the systematic status of *Leptocleidus* Andrews, 1922. Zootaxa 1863:1-120.

Everhart, M. J. 2005. Elasmosaurid remains from the Pierre Shale (Upper Cretaceous of western Kansas. Possible missing elements of the type specimen of *Elasmosaurus platyurus* Cope, 1868? PalArch Vertebrate Palaeontology 4:19–32.

Feldmann R. M., G. A. Bishop, and T. W. Kammer. 1977. Macrurous Decapods from the Bearpaw Shale (Cretaceous: Campanian) of Northeastern Montana. Journal of Paleontology 51:1161–1180.

Feldmann R. M., A. Frantescu, O. D. Frantescu, A. A. Klompmaker, G. Logan, C. M. Robins, C. E. Schweitzer, and D. A. Waugh. 2012. Formation of lobster-bearing concretions in the Late Cretaceous Bearpaw Shale, Montana, United States, in a complex geochemical environment. Palaios 27:842–856.

Gasparini, Z., N. Bardet, J. E. Martin, and M. Fernandez. 2003. The elasmosaurid plesiosaur *Aristonectes* Cabrera from the latest Cretaceous of South America and Antarctica. Journal of Vertebrate Paleontology 23:104–115.

Großmann, F. 2007. The taxonomic and phylogenetic position of the Plesiosauroidea from the Lower Jurassic Posidonia Shale of south-west Germany. Palaeontology 50:545–564.

Hampe, O. 2013. The forgotten remains of a leptocleidid plesiosaur (Sauropterygia: Plesiosauroidea) from the Early Cretaceous of Gronau (Münsterland, Westphalia, Germany). Paläontologische Zeitschrift 87:473–491.

He, S., T. K. Kyser, and W. G. E. Caldwell. 2005. Paleoenvironment of the Western Interior Seaway inferred from $\delta^{18}O$ and δ^{13} C values of molluscs from the Cretaceous Bearpaw marine cyclothem. Paleogeography, Paleoclimatology, and Paleoecology 217:67–85.

Hector, J. 1874. On the fossil reptiles of New Zealand. Transactions of the New Zealand Institute 6:333–358.

Hiller, N., A. A. Mannering, C. M. Jones, and A. R. I. Cruickshank. 2005. The nature of *Mauisaurus haasti* Hector, 1874 (Reptilia: Plesiosauria). Journal of Vertebrate Paleontology 25:588–601.

Hiller, N., J. P. O'Gorman, and R. A. Otero. 2014. A new elasmosaurid plesiosaur from the lower Maastrichtian of North Canterbury, New Zealand. Cretaceous Research 50:318–331.

ICZN, 1999. International Code of Zoological Nomenclature, fourth edition. International Trust for Zoological Nomenclature, The Natural History Museum, London, U.K. 306 pp.

Kauffman, E. G. 1984. Paleobiogeography and evolutionary response dynamic in the Cretaceous Western Interior Seaway of North America; pp. 273–306 in Westermann, G. E. G. (ed.), Jurassic–Cretaceous Paleogeography of North America. Geological Association of Canada Special Paper 27.

Kauffman, E. G., B. B. Sageman, J. I. Kirkland, W. P. Elder, P. J. Harries, and T. Villamil. 1993. Molluscan biostratigraphy of the Cretaceous Western Interior Basin, North America. Geological Association of Canada Special Papers 39:397–434.

Kear, B. P. 2005. A new elasmosaurid plesiosaur from the Lower Cretaceous of Queensland, Australia. Journal of Vertebrate Paleontology 25:792–805.

Ketchum, H. F., and R. B. J. Benson. 2010. Global interrelationships of Plesiosauria (Reptilia, Sauropterygia) and the pivotal role of taxon sampling in determining the outcome of phylogenetic analysis. Biological Reviews 85:361–392.

Ketchum, H. F., and R. B. J. Benson. 2011a. The cranial anatomy and taxonomy of *Peloneustes philarchus* (Sauropterygia, Pliosauridae) from the Peterborough Member (Callovian, Middle Jurassic) of the United Kingdom. Palaeontology 54:639–665.

Ketchum, H. F., and R. B. J. Benson. 2011b. A new pliosaurid (Sauropterygia, Plesiosauria) from the Oxford Clay Formation (Middle Jurassic, Callovian) of

England: evidence for a gracile, longirostrine grade of Early–Middle Jurassic pliosaurids. Palaeontology 86:109–129.

Kubo, T., M. T. Mitchell, and D. M. Henderson. 2012. *Albertonectes vanderveldei*, a new elasmosaur (Reptilia, Sauropterygia) from the Upper Cretaceous of Alberta. Journal of Vertebrate Paleontology 32:557–572.

Larson, N. L., and N. H. Landman. 2007. The geological and paleontological contributions of William 'Bill' A. Cobban. The Journal of Paleontological Sciences 7:1–46.

Leckie, R. M., M. G. Schmidt, D. Finkelstein, and R. Yuretich. 1991. Paleoceanographic and paleoclimatic interpretations of the Mancos Shale (Upper Cretaceous), Black Mesa Basin, Arizona. Geological Society of America Special Paper 260:139–152.

Lomax, D. R., and W. R. Wahl. 2013. A new specimen of the elasmosaurid plesiosaur *Zarafasaura oceanis* from the Upper Cretaceous (Maastrichtian) of Morocco. Paludicola 9:97–109.

Mulder, E. W. A., N. Bardet, P. Godefroit, and J. W. M. Jagt. 2000. Elasmosaur remains from the Maastrichtian type area, and a review of latest Cretaceous elasmosaurs (Reptilia, Plesiosauroidea). Bulletin de l'Institut Royal des Sciences Naturalles de Belgique, Sciences de la Terre 70:161–178.

Nixon, K. C. 1999. The Parsimony Ratchet, a new method for rapid parsimony analysis. Cladistics 15:407–414.

O'Gorman, J. P. 2016a. A small body sized non-aristonectine elasmosaurid (Sauropterygia: Plesiosauria) from the Late Cretaceous of Patagonia with

comments on the relationships of the Patagonian and Antarctic elasmosaurids. Ameghiniana 53:245–268.

O'Gorman, J. P. 2016b. Reappraisal of *Fresnosaurus drescheri* (Plesiosauria; Elasmosauridae) from the Maastrichtian Moreno Formation, California, U.S.A. Cretaceous Research 68:9-20.

O'Gorman, J. P., E. Olivero, and D. A. Cabrera. 2012. Gastroliths associated with a juvenile elasmosaur (Plesiosauria, Elasmosauridae) from the Snow Hill Island Formation (upper Campanian-lower Maastrichtian), Vega Island, Antarctica. Alcheringa 36:531–541.

O'Gorman, J. P., L. Salgado, E. B. Olivero, and S. A. Marenssi. 2015. *Vegasaurus molyi*, gen. et sp. nov. (Plesiosauria, Elasmosauridae), from the Cape Lamb Member (lower Maastrichtian) of the Snow Hill Island Formation, Vega Island, Antarctica and remarks on Wedellian Elasmosauridae. Journal of Vertebrate Paleontology 35:3, e931285, DOI:10.1080/02724634.2014.931285.

O'Keefe, F. R. 2001. A cladistics analysis and taxonomic revision of the Plesiosauria (Reptilia: Sauropterygia). Acta Zoologica Fennica 213:1-63.

O'Keefe, F. R., and M. T. Carrano. 2005. Correlated trends in the evolution of the plesiosaur locomotor system. Paleobiology 31:656–675.

O'Keefe, F. R., and N. Hiller. 2006. Morphologic and ontogenetic patterns in elasmosaur neck length, with comments on the taxonomic utility of neck length variables. Paludicola 5:206–229.

O'Keefe, F. R., and H. P. Street. 2009. Osteology of the cryptocleidoid plesiosaur *Tatenectes laramiensis*, with comments on the taxonomic status of the Cimoliasauridae. Journal of Vertebrate Paleontology 29:48-57.

Osborn, H. F. 1903. The reptilian subclasses Diapsida and Synapsida and the early history of the Diaptosauria. Memoir of the American Natural History 1:449–507.

Otero, R. A. 2016. Taxonomic reassessment of *Hydralmosaurus* as *Styxosaurus*: new insights on the elasmosaurid neck evolution throughout the Cretaceous. PeerJ 4:1–60.

Otero, R. A., S. Soto-Acuña, and D. Rubilar-Rogers. 2012. A postcranial skeleton of an elasmosaurid plesiosaur from the Maastrichtian of central Chile, with comments on the affinities of Late Cretaceous plesiosauroids from the Weddellian Biogeographic Province. Cretaceous Research 37:89–99.

Otero, R. A., S. Soto-Acuña, F. R. O'Keefe, J. P. O'Gorman, W. S. Stinnesbeck, M. E. Suárez, D. Rubilar-Rogers, C. Salazar, and L. A. Quinzio-Sinn. 2014a. *Aristonectes quiriquinensis* sp. nov., a new highly derived elasmosaurid from the upper Maastrichtian of central Chile. Journal of Vertebrate Paleontology 34:100-125.

Otero, R. A., S. Soto-Acuña, A. O. Vargas, and D. Rubilar-Rogers. 2014b. A new postcranial skeleton of an elasmosaurid plesiosaur from the Upper Cretaceous of central Chile and reassessment of *Cimoliasaurus andium* Deecke. Cretaceous Research 50:318–331.

Otero, R. A., S. Soto-Acuña, C. Salazar, and J. L. Oyarzún. 2015. New elasmosaurids (Plesiosauria, Sauropterygia) from the Late Cretaceous of the Magallanes Basin,

Chilean Patagonia: evidence of a faunal turnover during the Maastrichtian along the Weddellian Biogeographic Province. 1–42.

Otero, R. A., J. P. O'Gorman, N. Hiller, F. R. O'Keefe, and R. E. Fordyce. 2016. *Alexandronectes zealandiensis*, gen. et sp. nov., a new aristonectine plesiosaur from the lower Maastrichtian of New Zealand. Journal of Vertebrate Paleontology DOI:10.1080/02724634.2015.1054494.

Owen, R. 1860. On the orders of fossil and Recent Reptilia, and their distribution in time. Report of the British Association for the Advancement of Science 29:153–166.

Palamarczuk S., and N. H. Landman. 2011. Dinoflagellate cysts from the upper Campanian Pierre Shale and Bearpaw shale of the U.S. Western Interior. Rocky Mountain Geology 46:137–164.

Sachs, S. 2004. Redescription of *Woolungasaurus glendowerensis* (Plesiosauria: Elasmosauridae) from the Lower Cretaceous of northeast Queensland. Memoirs of the Queensland Museum 49:713–731.

Sachs, S. 2005. Redescription of *Elasmosaurus platyurus* Cope 1868 (Plesiosauria: Elasmosauridae) from the Upper Cretaceous (lower Campanian) of Kansas, U.S.A. Paludicola 5:92–106.

Sachs, S., and B. P. Kear. 2015. Postcranium of the paradigm elasmosaurid plesiosaurian *Libonectes morgani* (Welles, 1949). Geological Magazine 152:694-710.

Sachs, S., B. P. Kear, and M. J. Everhart. 2013. Revised vertebral count in the 'longest-necked vertebrate' *Elasmosaurus platyurus* Cope 1868 and clarification of the

cervical-dorsal transition in Plesiosauria. PLoS ONE 8(8): e70877. doi:10.1371/journal.pone.0070877.

Sachs, S., J. Lindgren, and M. Siversson. 2016a. A partial plesiosaurian braincase from the Upper Cretaceous of Sweden; pp. 293–302 in Kear, B. P., J. Lindgren, J. H. Hurum, J. Milàn, and V. Vajda (eds.) Mesozoic Biotas of Scandinavia and its Arctic Territories. Geological Society, London, Special Publications 434.

Sachs, S., M. Wilmsen, J. Knüppe, J. Hornung, and B. P. Kear. 2016b. Cenomanian–Turonian marine amniote remains from the Saxonian Cretaceous Basin of Germany. Geological Magazine doi:10.1017/S0016756815001004.

Sato, T. 2002. Description of plesiosaurs (Reptilia: Sauropterygia) from the Bearpaw Formation (Campanian–Maastrichtian) and a phylogenetic analysis of the Elasmosauridae. PhD Thesis, University of Calgary 1–412.

Sato, T. 2003. *Terminonatator ponteixensis*, a new elasmosaur (Reptilia; Sauropterygia) from the Upper Cretaceous of Saskatchewan. Journal of Vertebrate Paleontology 23:89–103.

Sato, T., Y. Hasegawa, and M. Manabe. 2006. A new elasmosaurid plesiosaur from the Upper Cretaceous of Fukushima, Japan. Paleontology 49:467–484.

Sato, T., T. Konishi, R. Hirayama, and M. W. Caldwell. 2012. A review of the Upper Cretaceous marine reptiles from Japan. Cretaceous Research 37:319–340.

Sikes, D. S., and P. O. Lewis. 2001. Beta Software, Version 1. PAUPRat: PAUP Implementation of the Parsimony Ratchet. Distributed by the authors. Department of Ecology and Evolutionary Biology, University of Connecticut, Storrs.

Swofford, D. 2002. PAUP*. Phylogenetic Analysis Using Parsimony (* and Other Methods). Version 4.0b10. Sinauer Associates, Sunderland.

Tourtelot, H. A. 1962. Preliminary investigation of the geologic setting and chemical composition of the Pierre Shale Great Plains region. Geological Survey Professional Paper 390:69–72.

Vincent, P., N. Bardet, X. P. Suberbiola, B. Bouya, M. Amaghzaz, and S. Meslouh. 2011. *Zarafasaura oceanis*, a new elasmosaurid (Reptilia: Sauropterygia) from the Maastrichtian Phosphates of Morocco and the palaeobiogeography of latest Cretaceous plesiosaurs. Gondwana Research 19:1062–1073.

Wegner, T. 1914. *Brancasaurus brancai* n. g. n. sp., ein Elasmosauridae aus dem Wealden Westfalens; pp. 235–305 in F. Schoendorf (ed.), Branca-Festschrift. Gebrüder Bornträger, Berlin.

Welles, S. P. 1943. Elasmosaurid plesiosaurs, with description of new material from California and Colorado. University of California Memoirs 13:125–254.

Welles, S. P. 1949. A new elasmosaur from the Eagle Ford shale of Texas; systematic description. Fondren Science Series 1:1–28.

Welles, S.P. 1952. A review of the North American Cretaceous elasmosaurs. University of California Publications in Geological Sciences 29:47–143.

Welles, S. P. 1962. A new species of elasmosaur from the Aptian of Colombia and a review of Cretaceous plesiosaurs. University of California Publications in Geological Sciences, University of California Berkeley 44:1–96.

Wiffen, J., and W. L. Moisley. 1986. Late Cretaceous reptiles (Families Elasmosauridae and Pliosauridae) from the Mangahouanga Stream, North Island, New Zealand. New Zealand Journal of Geology and Geophysics 29:205–252.

Williston, S. W. 1890. A new plesiosaur from the Niobrara Cretaceous of Kansas. Transactions of the Kansas Academy of Science 13:107–111.

Submitted July 08, 2016; revisions received October 3, 2016; accepted October 31, 2016.

Handling editor: Robin O'Keefe.

FIGURE CAPTIONS

FIGURE 1. Map showing the discovery site (star) of MOR 3072 in the Charles M. Russell Wildlife Refuge (CMRWR), Phillips County, Montana, U.S.A. Outline indicates the CMRWR boundaries. [planned for 2/3 page width]

FIGURE 2. Skeleton of MOR 3072, holotype specimen of *Nakonanectes bradti* gen. et sp. nov. **A**, articulated skeletal map showing the extent of the concretionary block and approximate positions of elements within the block. **B**, photo of the concretion and articulated cervical vertebrae taken at the time of discovery. Hatch marks indicate the portion of the skeleton lost to erosion prior to collection; cross hatching represents the poorly preserved posterior portion of the concretion. **Abbreviations: cdv**, caudal vertebrae; **cor**, coracoid; **cr**, cervical rib; **cv#**, cervical vertebra number; **dr**, dorsal rib;

dv, dorsal vertebrae; **f**, femur; **h**, humerus; **il**, ilium; **ph**, phalanx; **pu**, pubis; **r**, radius; **rf**, rib facet; **ti**, tibia; **u**, ulna. [planned for page width]

FIGURE 3. Cranium of MOR 3072, holotype specimen of *Nakonanectes bradti* gen. et sp. nov. **A**, laser scan and **B**, interpretation in left dorsolateral view. Cross-hatching indicates damaged area. **Abbreviations: a**, angular; **at-ax**, atlas-axis; **bs**, basisphenoid; **cv#**, cervical vertebra number; **d,** dentary; **en**, external naris; **eppt**, epipterygoid; **exop**, exoccipital-opisthotic; **f**, frontal; **j**, jugal; **mx**, maxilla; **or**, orbit; **p**, parietal; **pmx**, premaxilla; **po**, postorbital; **pof**, postfrontal; **pr**, prootic; **prf**, prefrontal; **q**, quadrate; **rap**, retroarticular process; **sa**, surangular; **scl**, scleral ring fragments; **soc**, supraoccipital; **sq**, squamosal. [planned for page width]

FIGURE 4. Cranium of MOR 3072, holotype specimen of *Nakonanectes bradti* gen. et sp. nov. **A**, laser scan and **B**, interpretation in right ventrolateral view. Dashed line indicates location of coronoid process. **Abbreviations: a**, angular; **ar**, articular; **at-ax**, atlas-axis; **bo**, basioccipital; **cp**, coronoid process; **cv#**, cervical vertebra number; **d**, dentary; **ecpt**, ectopterygoid; **j**, jugal; **mx**, maxilla; **or**, orbit; **pal**, palatine; **piv**, posterior interpterygoid vacuity; **pmx**, premaxilla; **po**, postorbital; **pra**, prearticular; **ps**, parasphenoid; **pt**, pterygoid; **q**, quadrate; **rap**, retroarticular process; **sa**, surangular; **sp**, splenial; **sq**, squamosal; **stf**, supratemporal fenestra. [planned for page width]

FIGURE 5. Detailed palatal view of MOR 3072, holotype specimen of *Nakonanectes bradti* gen. et sp. nov. **A**, photo and **B**, interpretation in right ventrolateral view. Cross

hatching represents damaged or covered areas. **Abbreviations: a**, angular; **ar**, articular; **bo**, basioccipital; **d**, dentary; **ectp**, ectopterygoid; **for**, foramen; **Mc**, opening for Meckelian canal; **oc**, occipital condyle; **pal**, palatine; **piv**, posterior interpterygoid vacuity; **popr**, paraoccipital process; **pra**, prearticular; **ps**, parasphenoid; **psp**, parasphenoid process; **pt**, pterygoid; **q**, quadrate; **sa**, surangular; **sp**, splenial; **sq**, squamosal. [planned for 2/3 page width]

FIGURE 6. Hyoids of MOR 3072, holotype specimen of *Nakonanectes bradti* gen. et sp. nov. **A**, left and **B**, right hyoids in medial view. Anterior is to the left. [planned for column width]

FIGURE 7. Atlas-axis complex of MOR 3072, holotype specimen of *Nakonanectes bradti* gen. et sp. nov. in **A**, right lateral, **B**, anterior, **C**, posterior, and **D**, ventral views. **Abbreviations: atc**, atlantal centrum; **atic**, atlantal intercentrum; **atna**, atlantal neural arch; **atns**, atlantal neural spine; **atr**, atlantal rib; **axc**, axial centrum; **axns**, axial neural spine; **axr**, axial rib; **hyp**, hypophyseal ridge; **poz**, postzygapophysis. [planned for 2/3 page width]

FIGURE 8. Cervical vertebrae 4, 8, and 18 of MOR 3072, holotype specimen of *Nakonanectes bradti* gen. et sp. nov. in **A**, **D**, **G**, posterior, **B**, **E**, **H**, right lateral, and **C**, **F**, **I**, ventral views. **Abbreviations: gr**, groove; **nc**, neural canal; **ns**, neural spine; **pops**, posterior process of neural spine; **poz**, postzygapophysis; **prz**, prezygapophysis; **ru**, rugosity; **vr**, ventral ridge; **vn**, ventral notch. [planned for page width]

FIGURE 9. Articulated anterior dorsal vertebrae of MOR 3072, holotype specimen of *Nakonanectes bradti* gen. et sp. nov. in **A**, right lateral and **B**, anterior views. Dashed white lines indicate outline of the dorsal rib facet; cross-hatching indicates matrix. **Abbreviations: c**, centrum; **drf**, dorsal rib facet; **poz**, postzygapophysis; **prz**, prezygapophysis; **ns**, neural spine; **tp**, transverse process. [planned for column width]

FIGURE 10. Partially prepared block of articulated caudal vertebrae and phalanges of MOR 3072, holotype specimen of *Nakonanectes bradti* gen. et sp. nov. **A**, photo and **B**, interpretation of block, with vertebrae shaded gray; **C**, detailed view of two articulated anterior caudals. Dashed lines indicate broken edges. **Abbreviations: cdr**, caudal rib; **ch**, chevron; **chf**, chevron facet; **rd**, ridge; **rf**, rib facet. [planned for 2/3 page width]

FIGURE 11. Articulated left and right coracoids of MOR 3072, holotype specimen of *Nakonanectes bradti* gen. et sp. nov. in **A**, anterior and **B**, ventral views. Dashed lines indicate broken edges. **Abbreviations: icv**, intercoracoid vacuity; **vmp**, ventromedial process. [planned for 2/3 page width]

FIGURE 12. Right forelimb of MOR 3072, holotype specimen of *Nakonanectes bradti* gen. et sp. nov. in ventral view. **Abbreviations: ao**, accessory ossicles; **dc1–4**, distal carpals; **dr**, dorsal rib; **epf**, epipodial foramen; **h**, humerus; **int**, intermedium; **ph**, phalanx; **r**, radius; **re**, radiale; **u**, ulna; **ue**, ulnare; **I–V**, metacarpals. [planned for 2/3 page width]

FIGURE 13. Right ilium of MOR 3072, holotype specimen of *Nakonanectes bradti* gen. et sp. nov. in **A**, anterior, **B**, medial, **C**, dorsal, **D**, posterior, **E**, lateral, and **F** ventral views. For **C** and **F**, anterior is up. **Abbreviations: acf**, acetabular facet; **isf**, ischial facet; **srf**, sacral rib facet. [planned for 2/3 page width]

FIGURE 14. Left hind limb of MOR 3072, holotype specimen of *Nakonanectes bradti* gen. et sp. nov. in **A**, dorsal, **B**, ventral, **C**, proximal and **D**, preaxial views. **Abbreviations: adr**, adductor rugosity; **cap**, capitulum; **f**, femur; **fi**, fibula; **fif**, fibular facet; **paf**, preaxial articular facet; **ti**, tibia; **tr**, trochanter. [planned for page width]

FIGURE 15. Time calibrated, strict reduced consensus tree of Elasmosauridae based on an analysis of the full matrix after exclusion of the wildcard taxa *Eromangasaurus australis* and *Elasmosaurus platyurus* (A) and *Futabasaurus suzukii* (B). *Nakonanectes bradti* gen. et sp. nov. is deeply nested in a clade of long-necked styxosaurines. Bremer support values greater than 1 are given below the internodes. [planned for page width]

TABLE 1. Selected measurements (cm) of MOR 3072, holotype specimen of *Nakonanectes bradti* nov. gen. et sp. Individual vertebral measurements can be found in Supplementary Data Table S1.

Dimension	cm
Skull length	32.9
Preorbital length	10.8
Preserved neck length (1–23)	86
Estimated right humerus midline length*	39–41
Right humerus distal width	22
Right radius length	12.5
Right radius width	14.5
Right ulna length	13.5
Right ulna width	11.5
Right forelimb width epipodial row	26
Right forelimb width mesopodial row	28.5
Left femur midline length	30
Left femur distal width	17
Left femur proximal width	11
Right ilium length	22

Length of skull measured from anterior end of premaxilla to posterior end of occipital condyle; *based on field photos.

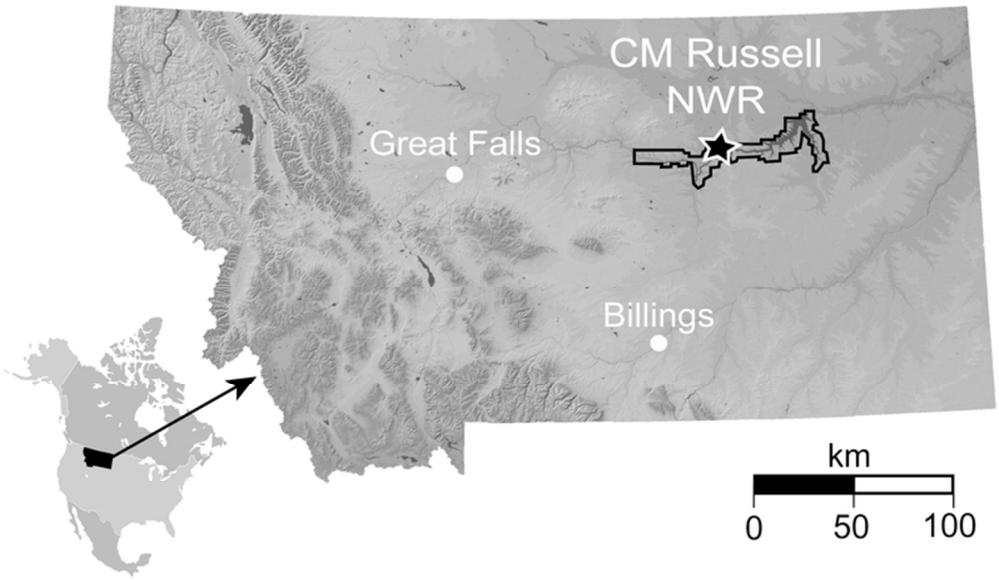

FIGURE 1. Map showing the discovery site (star) of MOR 3072 in the Charles M. Russell Wildlife Refuge (CMRWR), Phillips County, Montana, U.S.A. Outline indicates the CMRWR boundaries. [planned for 2/3 page width

67x39mm (300 x 300 DPI)

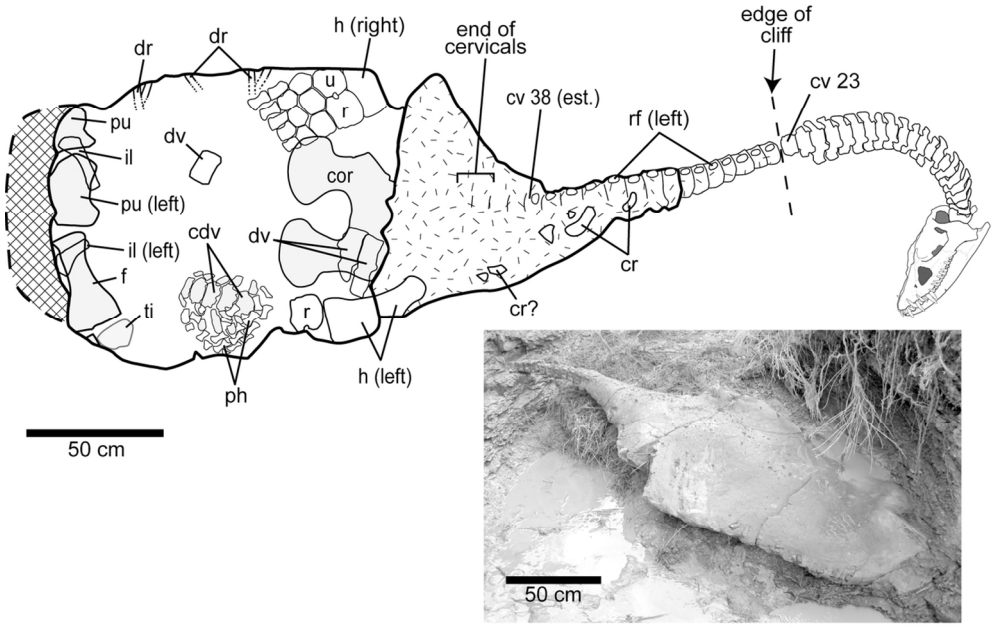

FIGURE 2. Skeleton of MOR 3072, holotype specimen of *Nakonanectes bradti* gen. et sp. nov. A, articulated skeletal map showing the extent of the concretionary block and approximate positions of elements within the block. B, photo of the concretion and articulated cervical vertebrae taken at the time of discovery. Hatch marks indicate the portion of the skeleton lost to erosion prior to collection; cross hatching represents the poorly preserved posterior portion of the concretion. Abbreviations: cdv, caudal vertebrae; cor, coracoid; cr, cervical rib; cv#, cervical vertebra number; dr, dorsal rib; dv, dorsal vertebrae; f, femur; h, humerus; il, ilium; ph, phalanx; pu, pubis; r, radius; rf, rib facet; ti, tibia; u, ulna. [planned for page width]

115x72mm (300 x 300 DPI)

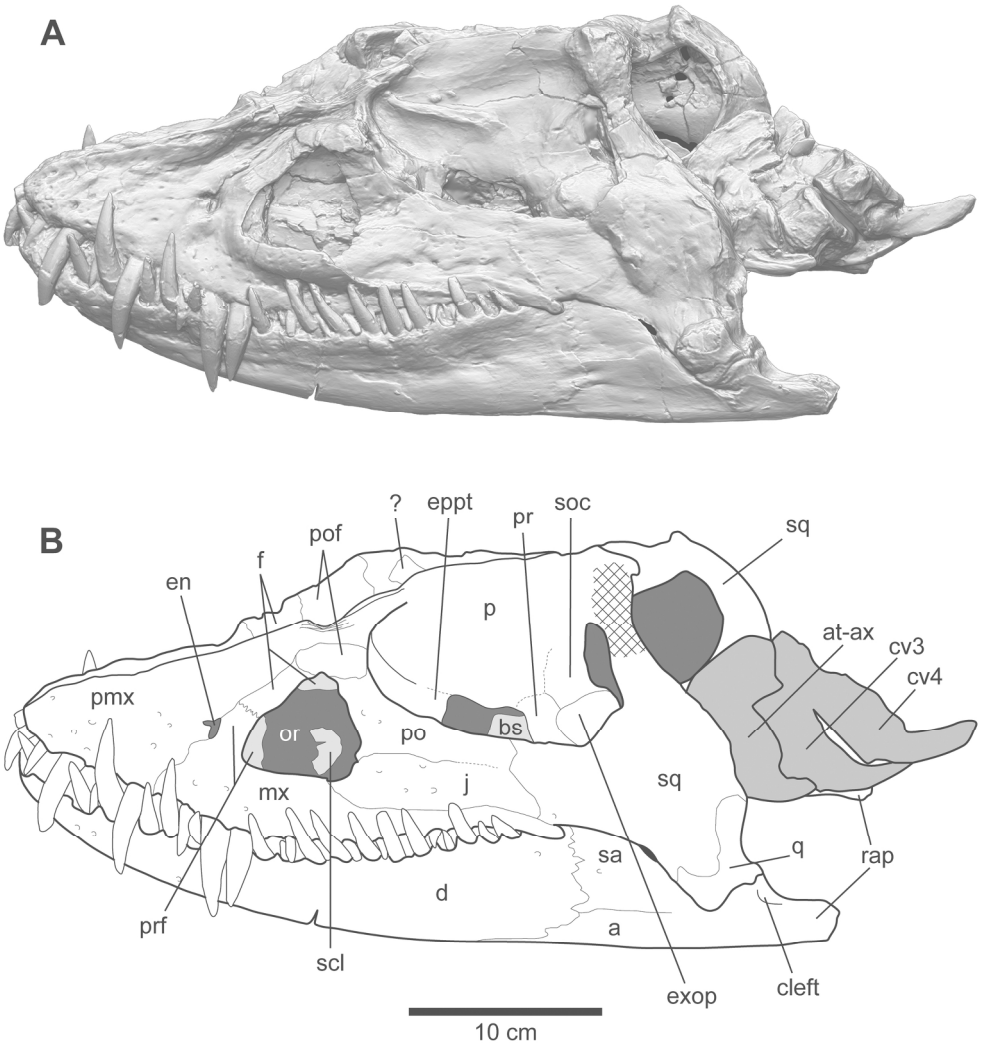

FIGURE 3. Cranium of MOR 3072, holotype specimen of *Nakonanectes bradti* gen. et sp. nov. A, laser scan and B, interpretation in left dorsolateral view. Cross-hatching indicates damaged area. Abbreviations: a, angular; at-ax, atlas-axis; bs, basisphenoid; cv#, cervical vertebra number; d, dentary; en, external naris; eppt, epipterygoid; exop, exoccipital-opisthotic; f, frontal; j, jugal; mx, maxilla; or, orbit; p, parietal; pmx, premaxilla; po, postorbital; pof, postfrontal; pr, prootic; prf, prefrontal; q, quadrate; rap, retroarticular process; sa, surangular; scl, scleral ring fragments; soc, supraoccipital; sq, squamosal. [planned for page width]

191x202mm (300 x 300 DPI)

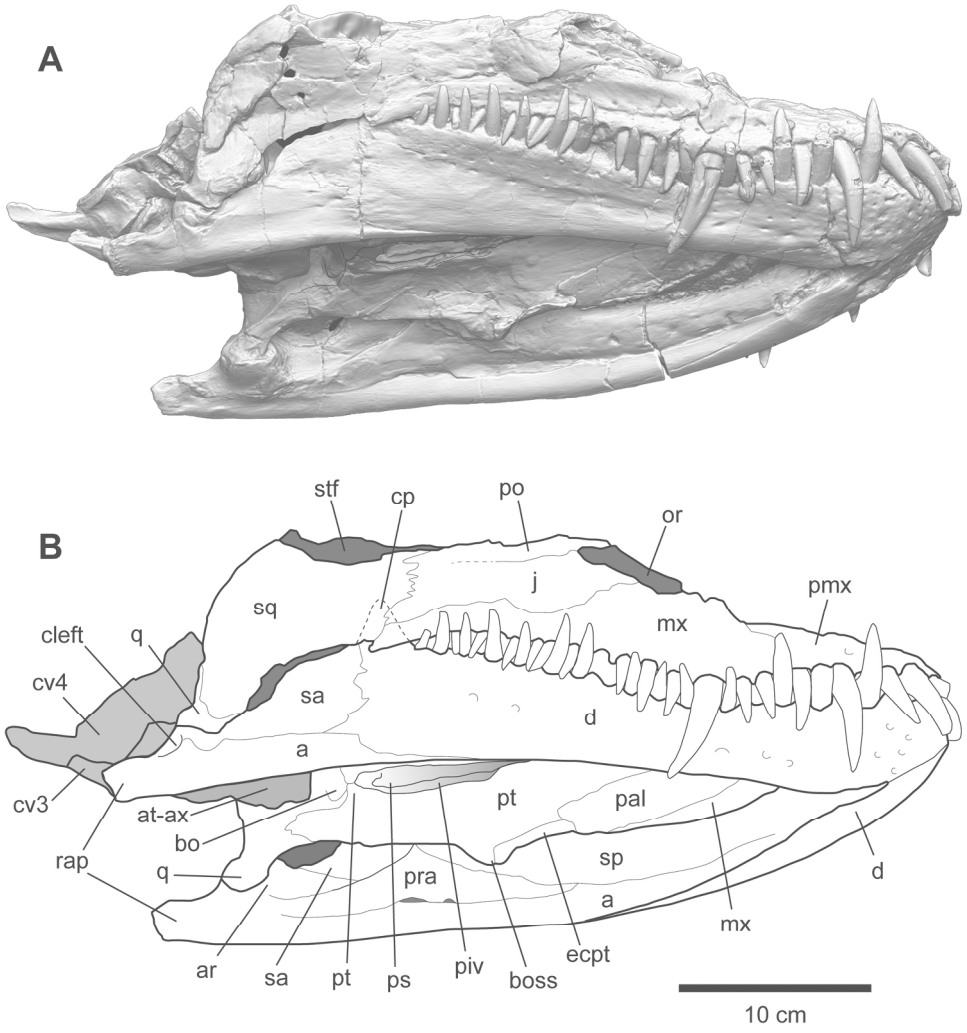

FIGURE 4. Cranium of MOR 3072, holotype specimen of *Nakonanectes bradti* gen. et sp. nov. A, laser scan and B, interpretation in right ventrolateral view. Dashed line indicates location of coronoid process. Abbreviations: a, angular; ar, articular; at-ax, atlas-axis; bo, basioccipital; cp, coronoid process; cv#, cervical vertebra number; d, dentary; ecpt, ectopterygoid; j, jugal; mx, maxilla; or, orbit; pal, palatine; piv, postrior interpterygoid vacuity; pmx, premaxilla; po, postorbital; pra, prearticular; ps, parasphenoid; pt, pterygoid; q, quadrate; rap, retroarticular process; sa, surangular; sp, splenial; sq, squamosal; stf, supratemporal fenestra. [planned for page width]

191x201mm (300 x 300 DPI)

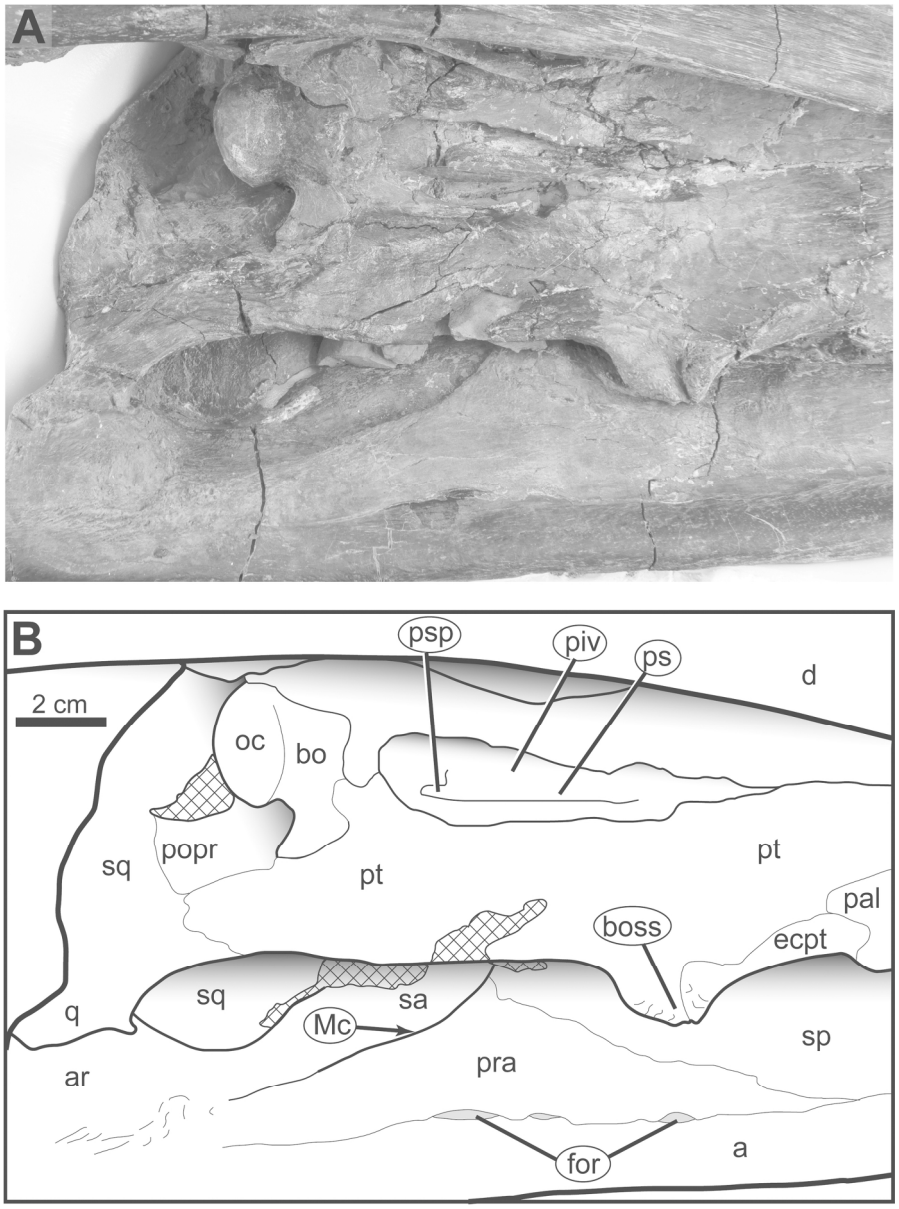

FIGURE 5. Detailed palatal view of MOR 3072, holotype specimen of *Nakonanectes bradti* gen. et sp. nov. A, photo and B, interpretation in right ventrolateral view. Cross hatching represents damaged or covered areas. Abbreviations: a, angular; ar, articular; bo, basioccipital; d, dentary; ectp, ectopterygoid; for, foramen; Mc, opening for Meckelian canal; oc, occipital condyle; pal, palatine; piv, posterior interpterygoid vacuity; popr, paraoccipital process; pra, prearticular; ps, parasphenoid; psp, parasphenoid process; pt, pterygoid; q, quadrate; sa, surangular; sp, splenial; sq, squamosal. [planned for 2/3 page width]

164x221mm (300 x 300 DPI)

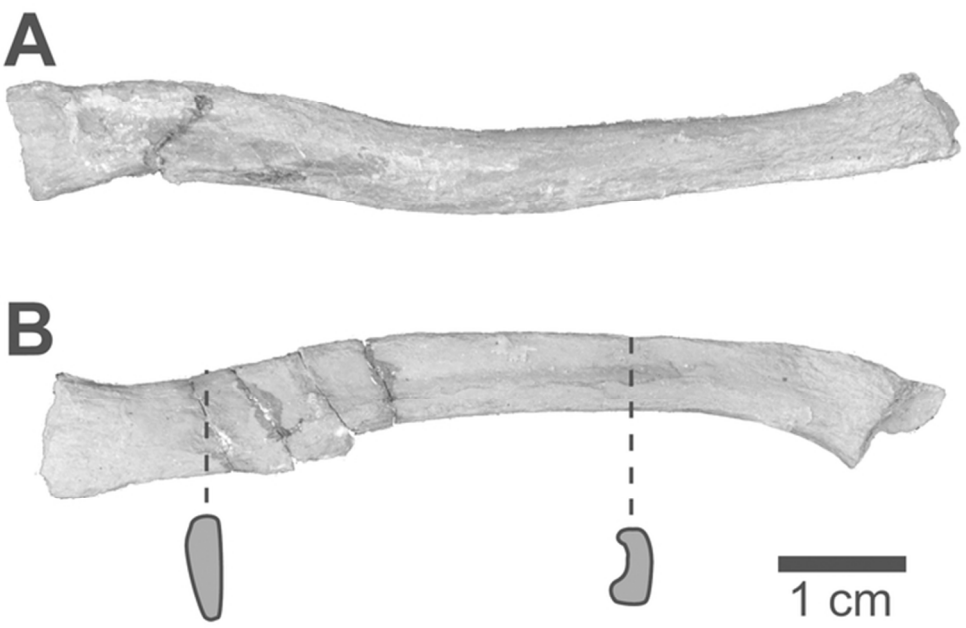

FIGURE 6. Hyoids of MOR 3072, holotype specimen of *Nakonanectes bradti* gen. et sp. nov. A, left and B, right hyoids in medial view. Anterior is to the left. [planned for column width]

60x41mm (300 x 300 DPI)

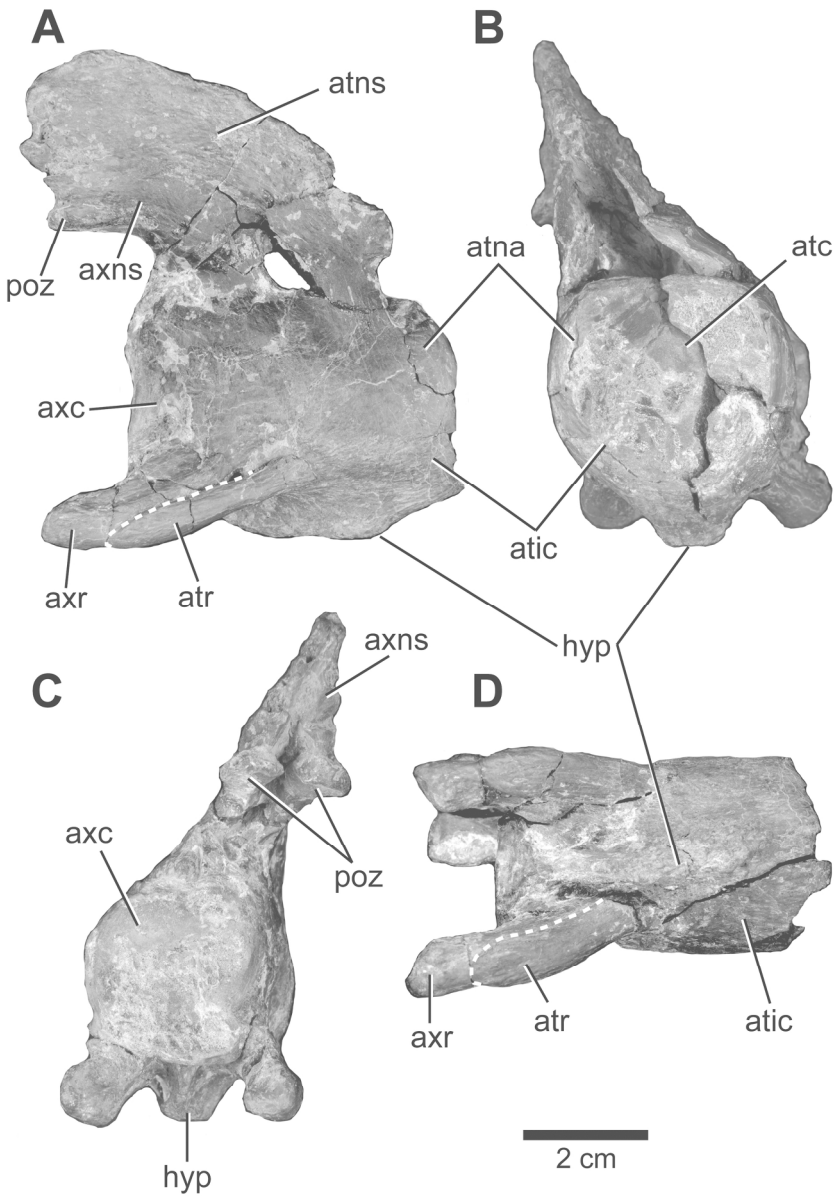

FIGURE 7. Atlas-axis complex of MOR 3072, holotype specimen of *Nakonanectes bradti* gen. et sp. nov. in A, right lateral, B, anterior, C, posterior, and D, ventral views. Abbreviations: atc, atlantal centrum; atic, atlantal intercentrum; atna, atlantal neural arch; atns, atlantal neural spine; atr, atlantal rib; axc, axial centrum; axns, axial neural spine; axr, axial rib; hyp, hypophyseal ridge; poz, postzygapophysis. [planned for 2/3 page width]

165x234mm (300 x 300 DPI)

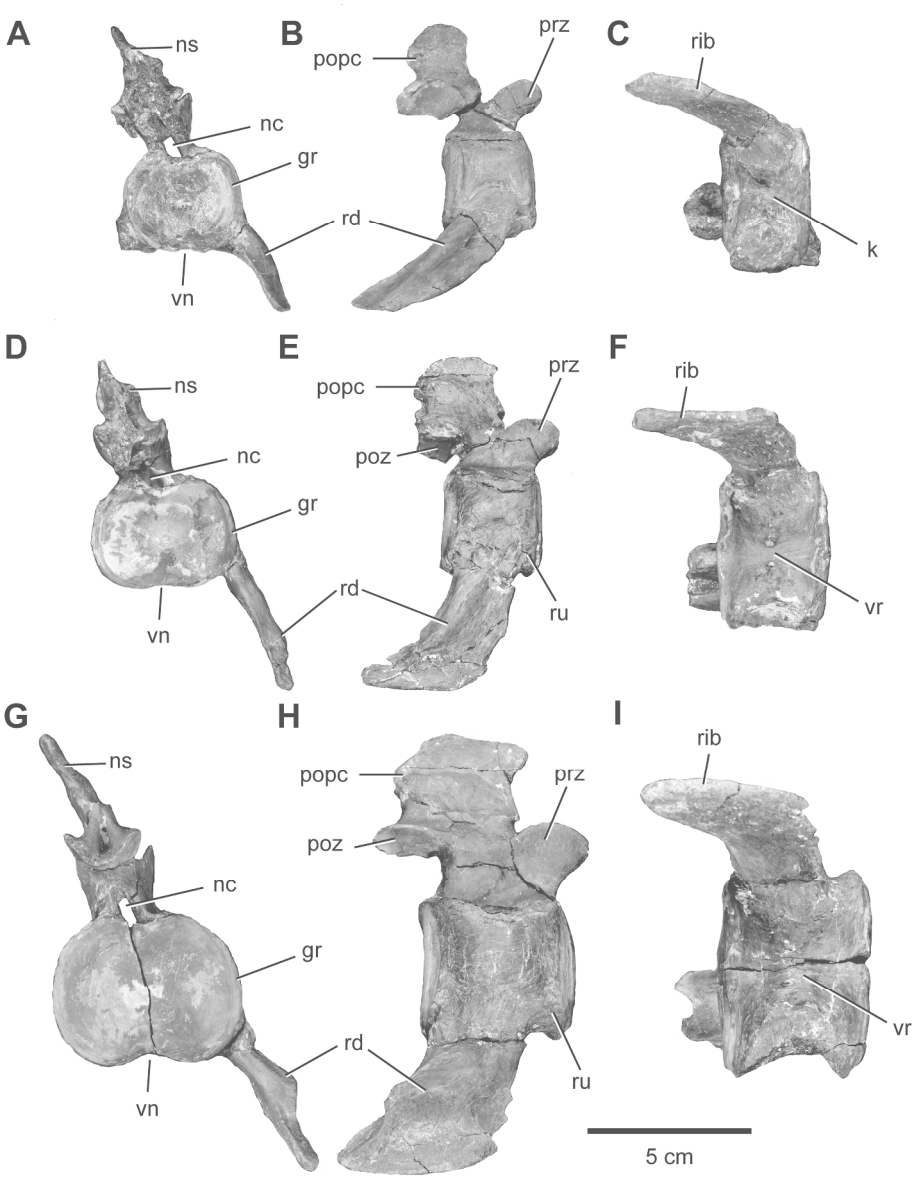

FIGURE 8. Cervical vertebrae 4, 8, and 18 of MOR 3072, holotype specimen of *Nakonanectes bradti* gen. et sp. nov. in A, D, G, posterior, B, E, H, right lateral, and C, F, I, ventral views. Abbreviations: gr, groove; nc, neural canal; ns, neural spine; pops, posterior process of neural spine; poz, postzygapophysis; prz, prezygapophysis; ru, rugosity; vr, ventral ridge; vn, ventral notch. [planned for page width]

228x291mm (300 x 300 DPI)

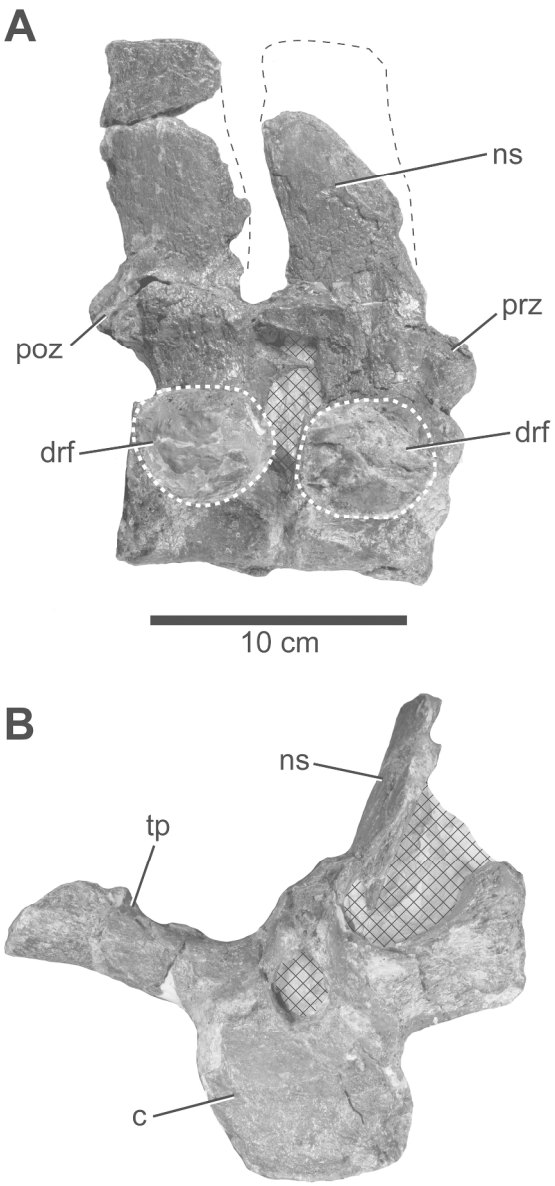

FIGURE 9. Articulated anterior dorsal vertebrae of MOR 3072, holotype specimen of *Nakonanectes bradti* gen. et sp. nov. in A, right lateral and B, anterior views. Dashed white lines indicate outline of the dorsal rib facet; cross-hatching indicates matrix. Abbreviations: c, centrum; drf, dorsal rib facet; poz, postzygapophysis; prz, prezygapophysis; ns, neural spine; tp, transverse process. [planned for column width]

172x342mm (300 x 300 DPI)

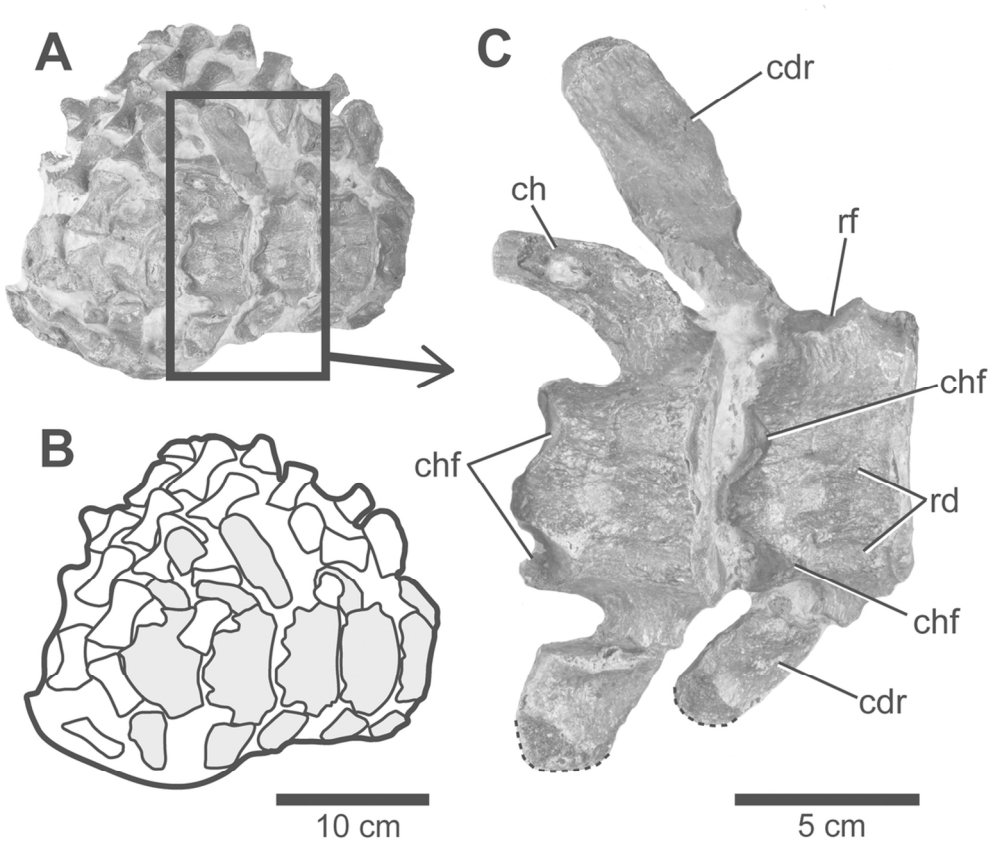

FIGURE 10. Partially prepared block of articulated caudal vertebrae and phalanges of MOR 3072, holotype specimen of *Nakonanectes bradti* gen. et sp. nov. A, photo and B, interpretation of block, with vertebrae shaded gray; C, detailed view of two articulated anterior caudals. Dashed lines indicate broken edges. Abbreviations: cdr, caudal rib; ch, chevron; chf, chevron facet; rd, ridge; rf, rib facet. [planned for 2/3 page width]

105x90mm (300 x 300 DPI)

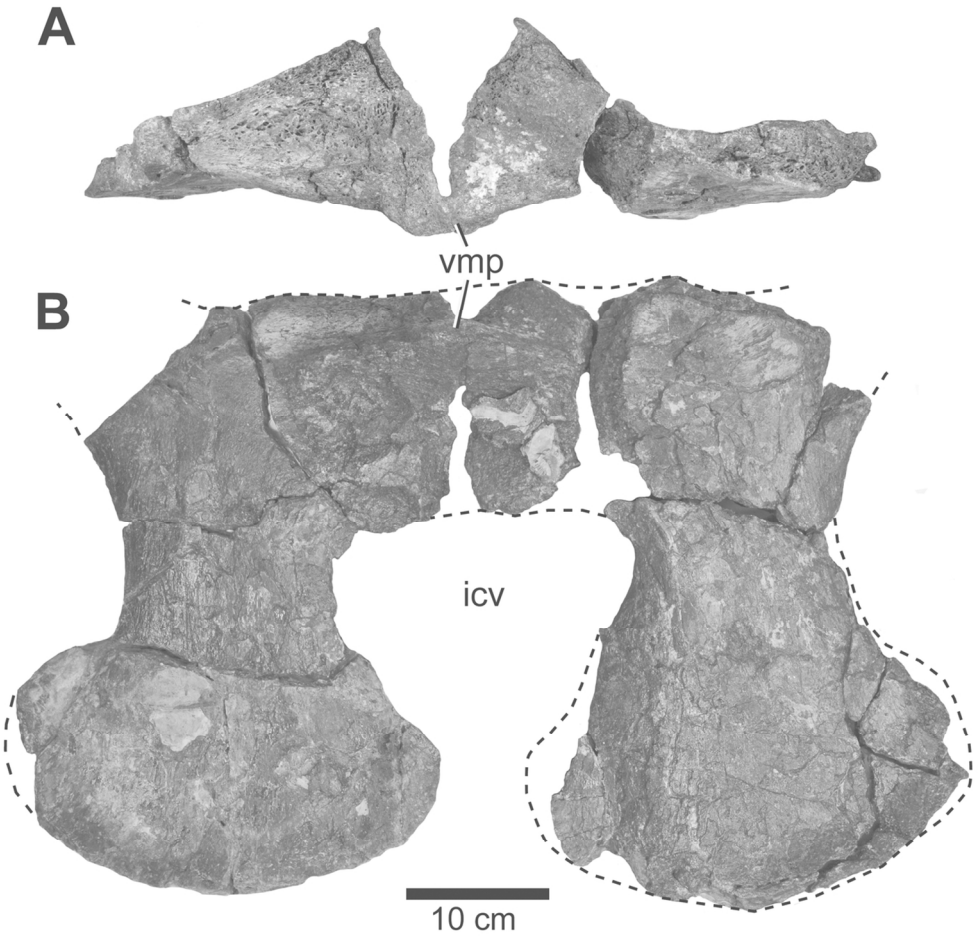

FIGURE 11. Articulated left and right coracoids of MOR 3072, holotype specimen of *Nakonanectes bradti* gen. et sp. nov. in A, anterior and B, ventral views. Dashed lines indicate broken edges. Abbreviations: icv, intercoracoid vacuity; vmp, ventromedial process. [planned for 2/3 page width]

116x110mm (300 x 300 DPI)

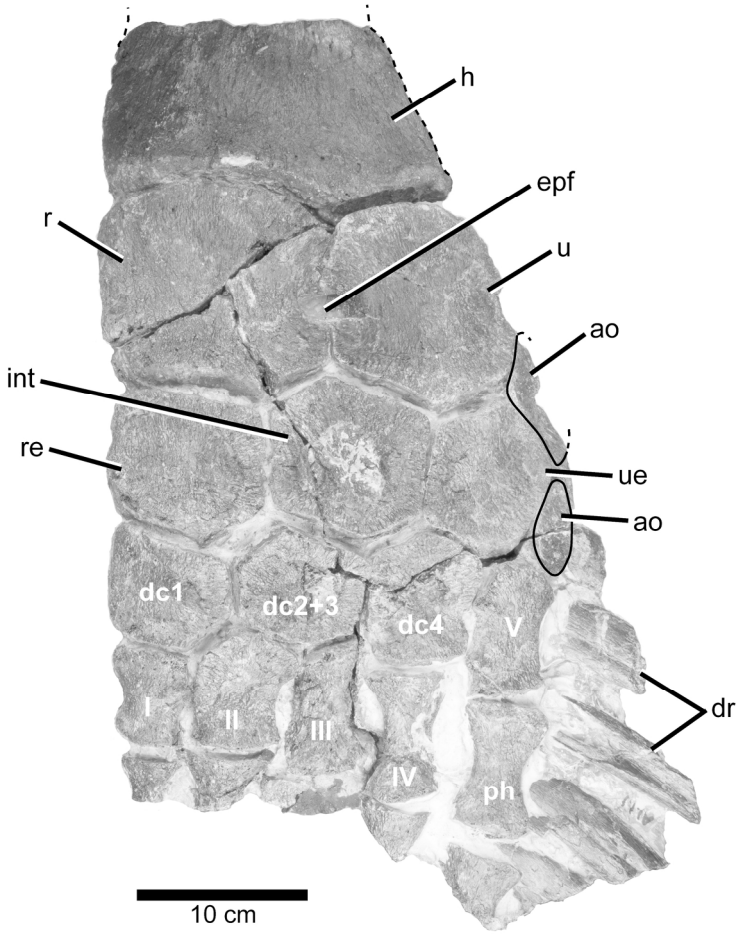

FIGURE 12. Right forelimb of MOR 3072, holotype specimen of *Nakonanectes bradti* gen. et sp. nov. in ventral view. Abbreviations: ao, accessory ossicles; dc1–4, distal carpals; dr, dorsal rib; epf, epipodial foramen; h, humerus; int, intermedium; ph, phalanx; r, radius; re, radiale; u, ulna; ue, ulnare; I–V, metacarpals.

185x219mm (300 x 300 DPI)

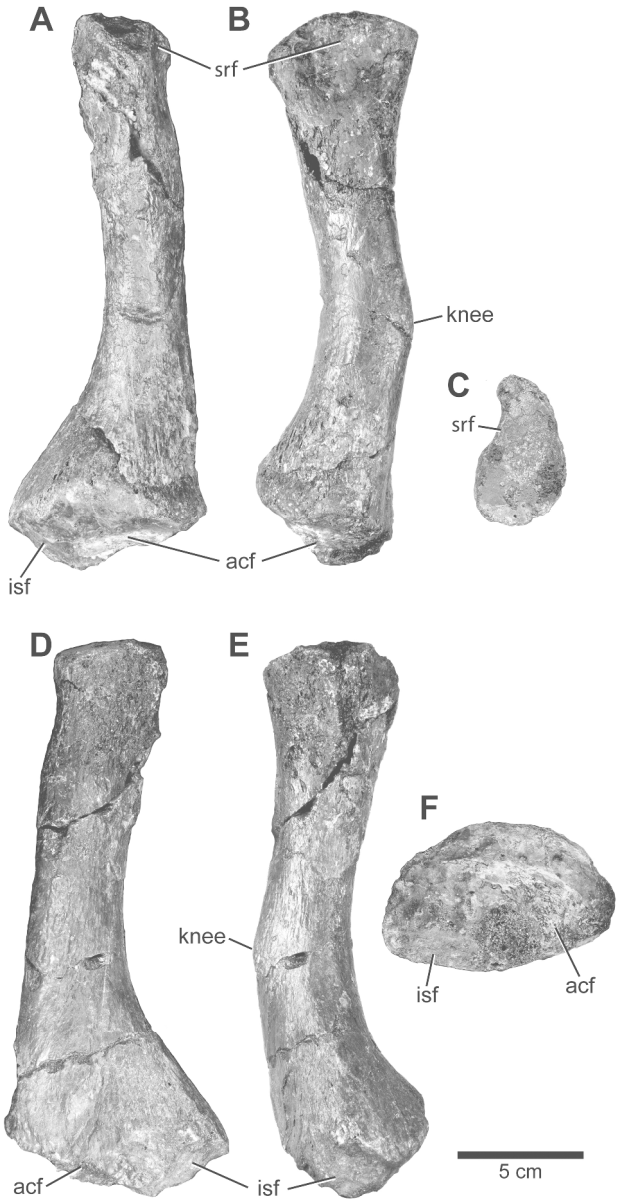

FIGURE 13. Right ilium of MOR 3072, holotype specimen of *Nakonanectes bradti* gen. et sp. nov. in A, anterior, B, medial, C, dorsal, D, posterior, E, lateral, and F ventral views. For C and F, anterior is up. Abbreviations: acf, acetabular facet; isf, ischial facet; srf, sacral rib facet. [planned for 2/3 page width]

230x447mm (300 x 300 DPI)

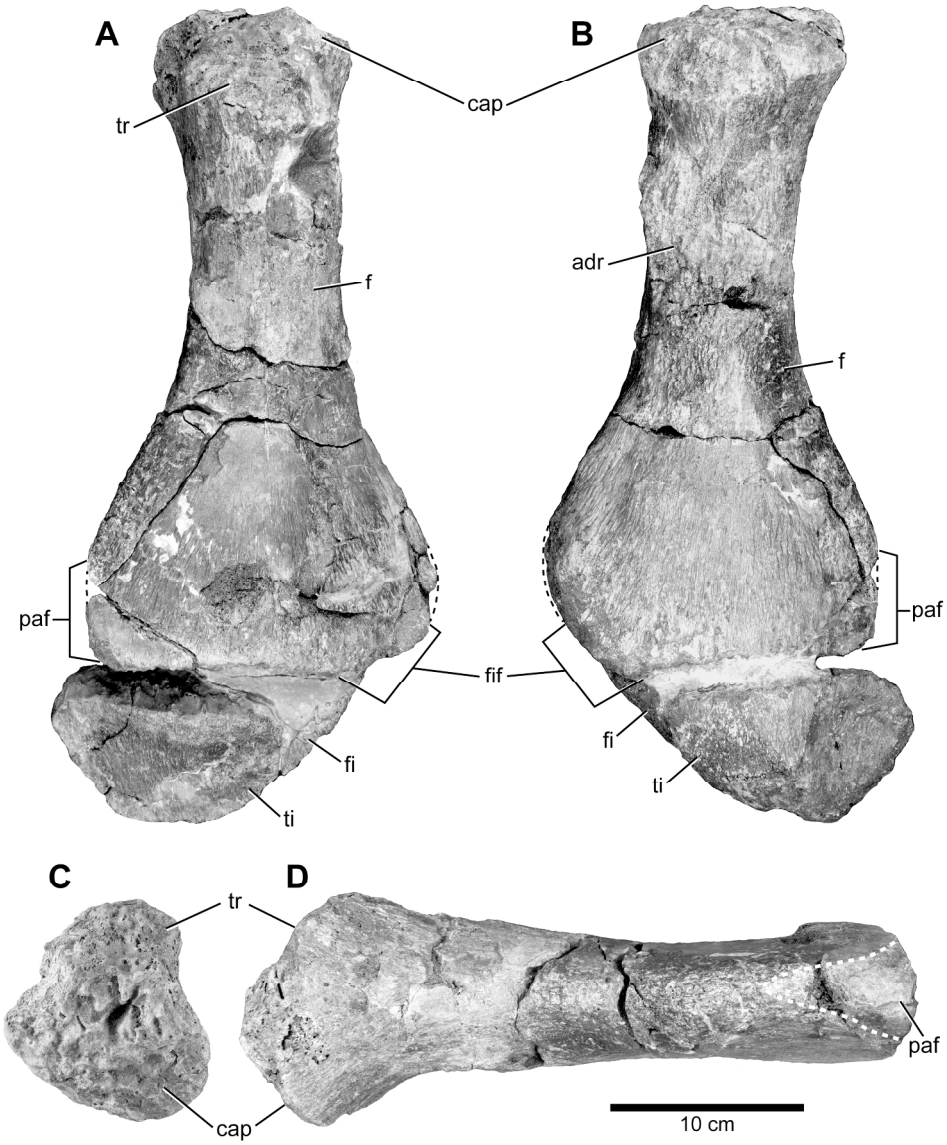

FIGURE 14. Left hind limb of MOR 3072, holotype specimen of *Nakonanectes bradti* gen. et sp. nov. in A, dorsal, B, ventral, C, proximal and D, preaxial views. Abbreviations: adr, adductor rugosity; cap, capitulum; f, femur; fi, fibula; fif, fibular facet; paf, preaxial articular facet; ti, tibia; tr, trochanter.

228x275mm (300 x 300 DPI)

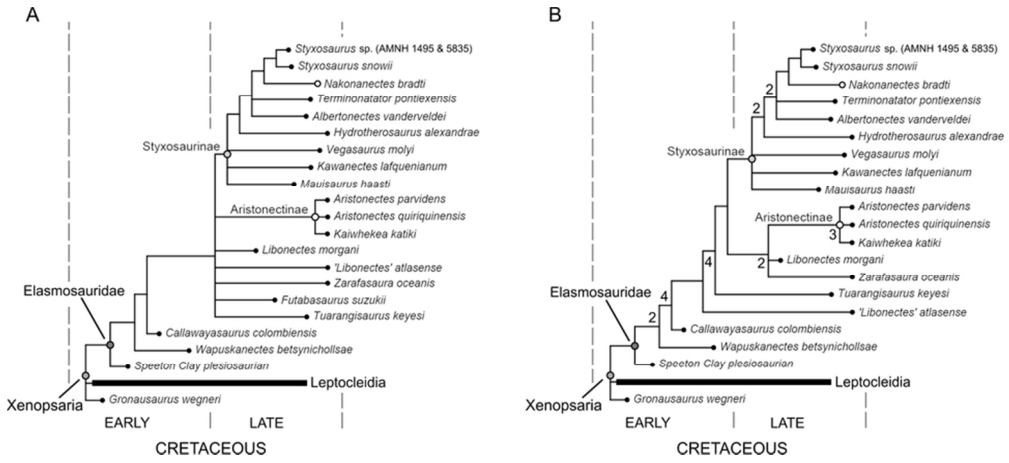

FIGURE 15. Time calibrated, strict reduced consensus tree of Elasmosauridae based on an analysis of the full matrix after exclusion of the wildcard taxa *Eromangasaurus australis* and *Elasmosaurus platyurus* (A) and *Futabasaurus suzukii* (B). *Nakonanectes bradti* gen. et sp. nov. is deeply nested in a clade of long-necked styxosaurines. Bremer support values greater than 1 are given below the internodes.

81x36mm (300 x 300 DPI)